FACULTY OF TEXTILE ENGINEERING TUL

THERMOELECTRIC BEHAVIOR OF COPPER-NICKEL COATED POLYETHYLENE TEREPHTHALATE FABRIC

Xiuling Zhang, M.Eng.

SUMMARY OF THE THESIS

Title of the thesis:	**Thermoelectric Behavior of Copper-Nickel Coated Polyethylene Terephthalate Fabric**
Author:	**Xiuling Zhang, M.Eng.**
Field of study:	**Textile Engineerig**
Mode of study:	**full time**
Department:	**Department of Material Engineering**
Supervisor:	**doc. Dr. Ing. Dana Křemenáková**

Composition of the dissertation defense committee:

Chairman: doc. Ing. Jiří Chvojka, Ph.D.	FT TUL, Department of Nonwovens and Nanofibrous Materials
Vice-chairmain: prof. Ing. Luboš Hes, DrSc., Dr.h.c.	
prof. Ing. Dr. Čestmír Drašar (opponent)	University of PardubiceFaculty of Chemical Technology – CEMNAT
doc. Ing. Veronika Tunáková, Ph.D.	FT TUL, Department of Material Engineering
Ing. Karel Kupka, PhD. (opponent)	TriloByte Statistical Software, s.r.o.
Ing. Miroslava Pechočiaková, Ph.D.	FT TUL, Department of Material Engineering
Ing. Blanka Tomková, Ph.D.	FT TUL, Department of Material Engineering

The dissertation can be consulted at the Department of Doctoral Studies, Faculty of Textiles, Technical University of Liberec.

Liberec 2025

Abstract

Textile-based thermoelectric materials are increasingly recognized for their potential in wearable electronics, offering flexibility, breathability, and energy harvesting capabilities. However, achieving high thermoelectric performance alongside mechanical durability and stability remains a critical challenge. In this thesis, nickel (Ni)-coated and copper (Cu)-coated polyester nonwoven fabrics (Ni@Cu-coated fabrics) were successfully fabricated using a combination of chemical plating and electroplating techniques. The copper layer was initially formed by chemical plating, followed by electroplating, while the nickel deposition was precisely controlled by adjusting the electroplating time. Comprehensive characterization, including morphological, compositional, and structural analyses, was conducted to evaluate the samples.

Morphological analysis revealed that the nickel layer gradually covered the copper layer and filled the fabric pores with increasing electroplating time, forming nanoscale, uniform, and compact coatings. Structural and valence state analysis identified copper oxides predominantly in the chemical plating region and nickel oxides in the nickel layer, both of which were found to enhance the material's thermoelectric performance. Compared to conventional nickel electroplating on copper foils, the Ni@Cu-coated fabrics significantly reduced short-circuit risks, attributed to the nanoscale distribution of metal particles and the stabilizing effect of copper oxides on electrical conductivity.

To evaluate thermoelectric performance, two testing setups were developed: a continuous cooling model for broad temperature ranges (11.5 °C to 110 °C) and a controlled temperature model for precise testing (14 °C to 62 °C). Both methods demonstrated strong consistency, validating the reliability of the continuous cooling approach. The Seebeck coefficient remained stable within the range of 8.75 to 17.50 μV/K across wide temperature differences. The material demonstrated rapid thermoelectric response, with time constants ($t_{0.63}$ and $t_{0.93}$) of 2.5 seconds and 4 seconds, respectively, under a 5 °C temperature difference. The fabrics also exhibited stable performance under twisting, wind exposure, and after washing.

In addition to thermoelectric performance, the Ni@Cu-coated fabrics displayed superior breathability, electromagnetic shielding, and low thermal conductivity, making them ideal for smart flexible thermocouple applications. This work provides a scalable and practical strategy for designing high-performance textile-based thermoelectric materials, paving the way for advanced wearable energy solutions.

Keywords:
Thermoelectric property, PET, fibrous material, Copper, Nickel, electroplating, Seebeck coefficient

Anotace

Textilní termoelektrické materiály získávají stále větší význam pro svoje možné aplikace v oblasti nositelné elektroniky, díky své flexibilitě, prodyšnosti a schopnosti generovat elektrickou energii z tepelné energie. Přesto zůstává dosažení vysoké termoelektrické výkonnosti spolu s mechanickou odolností a stabilitou klíčovou výzvou. V této práci byly použity polyesterové netkané textilie úspěšně potažené niklem (Ni) a mědí (Cu) (Ni@Cu-coated fabrics) pomocí kombinace chemického pokovování a elektrolytické depozice. Měděná vrstva byla nejprve vytvořena chemickým pokovováním a následně elektrolyticky, přičemž depozice niklu byla přesně řízena úpravou doby elektrolytické depozice. Byla provedena komplexní charakterizace vzorků zahrnující analýzu složení, popis morfologie, a strukturální analýzu.

Morfologická analýza vedla k závěru, že nikl postupně pokrývá měděnou vrstvu a vyplňuje póry textilie se zvyšující se dobou elektrolytické depozice, přičemž vznikají nanoskopické, rovnoměrné a kompaktní vrstvy. Strukturální analýza a analýza valenčních stavů identifikovaly oxidy mědi převážně v oblasti chemického pokovování a oxidy niklu ve vrstvě niklu, přičemž bylo zjištěno, že obě tyto složky přispívají ke zlepšení termoelektrických vlastností materiálu. Ve srovnání s konvenčním elektrolytickým pokovováním niklem na měděné fólii se díky nanoskopické distribuci kovových částic a stabilizačnímu účinku oxidů mědi na elektrickou vodivost výrazně snížilo riziko zkratu.

Pro hodnocení termoelektrických vlastností byly vyvinuty dva testovací systémy: model kontinuálního chlazení pro široké teplotní rozsahy (11,5 °C až 110 °C) a model s regulovanou teplotou pro přesné testování (14 °C až 62 °C). Obě metody prokázaly silnou podobnost výsledků, což potvrzuje použitelnost kontinuálního chlazení. Seebeckův koeficient zůstal stabilní v rozmezí 8,75 až 17,50 μV/K při vysokých teplotních rozdílech. Materiál vykazoval rychlou termoelektrickou odezvu s časovými konstantami ($t_{0,63}$ a $t_{0,93}$) 2,5 sekundy a 4 sekundy při teplotním rozdílu 5 °C. Textilie si také zachovaly stabilní chování při krutu, vystavení větru a ostatním klimatickým faktorům (zejména vlhkosti) a po praní.

Kromě termoelektrických vlastností vykazovaly „Ni@Cu-coated fabrics“ vynikající flexibilitu, prodyšnost, elektromagnetické stínění a tepelný komfort, což je činí vhodnými pro aplikace v inteligentních nositelných textiliích. Tato práce prokazuje praktickou strategii pro navrhování vysoce výkonných textilních termoelektrických materiálů, otevírající cestu k pokročilým materiálům zajištujícím nositelné generátory elektrické energie z energie tepelné a naopak.

Klíčová slova: Termoelektrické jevy, PET netkaná textilie, Měď, Nikl, Elektrolytické pokovování, Seebeckův koeficient

.

Summary

1 Introduction

The Seebeck effect, first observed in 1774 and later studied extensively in 1821, refers to the generation of an electromotive force when a temperature difference is applied across a bimetallic material [1,2]. This fundamental thermoelectric phenomenon forms the basis for converting thermal energy into electrical energy and has broad applications, including temperature sensing [3–5], energy harvesting [6,7], and power generation [8,9]. Among these, thermocouples are fundamental components in temperature measurement systems and demonstrate the principles of thermoelectric conversion. As one of the most practical implementations of the Seebeck effect, thermocouples play a pivotal role in accurately measuring temperature by converting temperature gradients into measurable voltage, while thermoelectric generators use similar principles for energy conversion in power generation systems.

With the rapid development of portable and smart wearable electronics technology, embedding thermoelectric systems into flexible textile materials is receiving widespread attention [10–12]. Thermoelectric systems, such as thermocouples or thermopiles, embedded in flexible textile materials utilize the temperature difference between the human body and the external environment to enable various health monitoring functions, which have become a focus of growing interest [2]. For example, recent studies have employed metal wires in the form of thermocouples or thermopiles embedded in textiles for use as temperature and heat flux sensors [13,14]. However, traditional thermoelectric materials, typically metal wires, while possessing excellent thermoelectric properties, suffer from rigidity and poor flexibility，this limitation restricts their comfort and suitability for wearable applications [15]. Instead, there has been a growing interest in thermoelectric textiles (TETs), as they provide softness, flexibility, breathability , deformability and porosity features [16].

Typically, thermoelectric textiles (TETs) are fabricated by integrating thermoelectric materials with fibers, filaments, or fabrics by using screen printing [17–19], ink printing [20], vacuum filtration [21] and magnetron sputtering [22], electroplating [2,23]etc. Current fiber-based preparation methods are relatively limited. A comparison of the Seebeck coefficients obtained by various methods for preparing film-based thermoelectric materials reveals that magnetron sputtering offers better surface smoothness and thermoelectric properties than other techniques [24–27]. However, its production efficiency is very low. Therefore, achieving large-scale production of thermoelectric textiles while reducing costs remains a significant challenge [28].

The ideal TE material for TETs is expected to be lightweight, non-toxic, chemically and mechanically stable, flexible, stretchable, and capable of interacting effectively with traditional textile fibers [15,29]. Organic thermoelectric (TE) materials, such as polyacetylene (PA) [16], polyaniline (PANI) [30], poly(3,4-ethylenedioxythiophene) (PEDOT) [31], poly(3-hexylthiophene), Polypyrrole (PPy) [32] generally meet the requirements for flexibility and integration requirements. However, their low TE performance limits their practicality in real-life applications. In contrast, inorganic TE materials offer high TE performance but suffer from limited mechanical flexibility and poor compatibility with textile fibers.

Electroplating is an effective method for incorporating metals into thermoelectric textiles, having been used to deposit various metals, including Cu, Ni, and Ag, onto fibrous materials [2,23,33,34]. By partially depositing metal onto conductive fiber materials, thermoelectric textiles with junctions of two conductive materials can be fabricated. Studies on carbon-metal thermoelectric textiles

remain limited. For instance, Hardianto et al. [2] employed electroplating to coat carbon fibers with nickel (Ni), resulting in a textile-based thermocouple (TC) featuring a structure consisting of nickel-coated carbon fibers and bare carbon fibers and achieving an S value of around 13 μV/K. However, the deposition of nickel on carbon fibers takes 60 minutes, which limits the scale and efficiency of production. Theoretically, metal-to-metal thermoelectric textiles with high Seebeck coefficient differences (e.g. Ni/Cu) offer comparable performance and better cost-effectiveness, but studies on the fabrication of such metal-to-metal thermoelectric textiles using electroplating methods remain absent.

In this work, nickel (Ni)-coated copper (Cu)-coated polyester nonwoven fabrics (Ni@Cu-coated fabrics) were developed using electroplating technology, with the copper layer prepared through a combination of chemical plating and electroplating. The precise control of nickel deposition through electroplating resulted in nanoscale, uniform, and compact coatings. Comprehensive characterization revealed that the nickel layer gradually covered the copper layer and filled the fabric pores with increasing electroplating time, while the presence of copper and nickel oxides contributed positively to thermoelectric performance. The fabricated Ni@Cu-coated fabrics demonstrated stable Seebeck coefficients (8.75 to 17.50 μV/K) across a wide temperature range (11.5 °C to 110 °C) and reliable performance under various conditions, including twisting, wind exposure, and after washing. It also exhibited superior breathability and comfort, making them highly suitable for smart wearable applications.

2 Purpose and the aim of the thesis

The aim of this research is to develop an innovative copper (Cu)-nickel (Ni) coated polyethylene terephthalate (PET) nonwoven fabric using an electroplating method and to perform a comprehensive investigation of its thermoelectric properties, with a focus on its potential applications in smart wearable technologies.

To achieve this aim, the objective will focus on:

- Development and optimization of Ni@Cu-coated fabrics: To fabricate a multilayer thermoelectric material by electroplating nickel (Ni) onto a commercially available copper-coated non-woven fabric substrate. The base substrate features a chemically deposited copper ion layer (copper seed) followed by electroplated copper (Cu) particles. The process will focus on optimizing electroplating methods and solutions to achieve a stable, reproducible technique, with precise control over the nickel layer's deposition time to ensure consistent quality.

- Characterization of morphology, composition, structure, and chemical valence states: The Ni@Cu-coated PET fabrics will be thoroughly characterized to evaluate their surface morphology, chemical composition, crystalline structure, and chemical valence states. Advanced analytical techniques such as scanning electron microscopy (SEM), focused ion beam (FIB), energy-dispersive X-ray spectroscopy (EDX), X-ray diffraction (XRD), and X-ray photoelectron spectroscopy (XPS) will be employed. Special emphasis will be placed on analyzing the chemical valence states to gain a deeper understanding of the material's properties, with particular attention to potential copper oxides and their impact on performance.

- Characterization of thermoelectric (TE) behavior: The thermoelectric properties of the developed multilayer materials were evaluated using customized measuring equipment equipped with two temperature control models (continuous cooling model and a controlled temperature model). The focus was on the measurement of the Seebeck coefficient with special attention to its linearity in the low temperature range. The data will be used to develop a predictive model to accurately predict the thermoelectric behavior of the materials. The TE stability of Ni@Cu-coated PET fabrics will be evaluated under deformation, various environmental conditions, and after washing cycles. Additional properties, including electrical conductivity and EMI shielding, will be evaluated to investigate their possible impact on the material's thermoelectric behavior.

- Comprehensive evaluation of wearability and comfort: To comprehensively analyze and evaluate the sample fabric's air permeability, thermal conductivity and thermal resistance to ensure its suitability for practical applications.

3 Overview of the current state of the problem

The Seebeck effect was first observed by the Italian scientist Alessandro Volta in 1774, who noted the relationship between heat and electrical phenomena. Later, in 1821, Baltic-born German physicist Thomas Johann Seebeck independently rediscovered and systematically studied the effect, leading to it being named after him. The Seebeck effect is a thermoelectric phenomenon in which a temperature difference between the junctions of two different conductors or semiconductors drives the movement of charge carriers, such as electrons or holes, resulting in the generation of an electromotive force (EMF) or voltage.

The Seebeck effect plays a foundational role in thermoelectric energy generation and temperature sensing. It is the underlying principle behind thermoelectric generators (TEGs), which harness waste heat from industrial processes, automotive systems, and even body heat, converting it into usable electrical power [35]. Additionally, the Seebeck effect is critical in thermocouples, which provide precise temperature measurements for industrial, scientific**,** and medical applications.
Thermoelectric (TE) materials can basically be divided into two main categories: organic and inorganic materials. Inorganic TE materials excel in thermoelectric performance, they are typically optimized for operation at temperatures above 900 K, further limiting their practicality for low-temperature applications. On the other hand, organic thermoelectric materials have gained considerable attention in recent years due to their intrinsic flexibility, lightweight, and compatibility with textile substrates. However, despite these advantages, its thermoelectric performance remains lower than that of inorganic materials. Therefore, despite their advantages in flexibility and compatibility with textile substrates, the thermoelectric properties of organic conducting polymers are ultimately constrained by their inherent limitations, such as low electrical conductivity and Seebeck coefficients.

To overcome these challenges, researchers are actively investigating hybrid approaches that integrate the superior thermoelectric performance of inorganic materials with the inherent flexibility and compatibility of organic materials. This synergy offers a promising pathway for the development of advanced textile-based thermoelectric materials, enabling efficient harvesting of body heat for power generation and precise temperature sensing in wearable applications.
The development of thermoelectric textiles has led to the emergence of diverse structures, which can generally be classified into two main categories: one-dimensional fibers/yarns and two-dimensional fabrics. One-dimensional thermoelectric textiles, with substrates based on yarns, filaments, or fibers, have gained research attention for their inherent flexibility and potential for seamless integration into textiles. In contrast, two-dimensional thermoelectric textiles, constructed from various fabric structures such as knitted, woven, nonwoven, or braided materials, offer advantages such as larger surface area coverage, mechanical stability, and ease of integration with other functional components, making them highly suitable for broader applications.

Building upon the characteristics of linear thermoelectric fibers and yarns, planar thermoelectric textiles offer distinct advantages that address some limitations of their linear counterparts. While linear materials are effective for localized thermoelectric conversion, their applications can be constrained by mechanical challenges and limited surface coverage. Planar thermoelectric textiles, such as knitted, woven, or nonwoven fabrics, provide broader functionality and adaptability,

making them ideal for larger-scale and more versatile applications.

The structural integrity of planar fabrics ensures a uniform distribution of thermoelectric performance across a larger area, aligning well with existing textile processing techniques (e.g., cutting, layering). This compatibility facilitates large-scale production and seamless integration into wearable systems. By contrast, one-dimensional materials often require additional assembly steps to achieve similar functionality.

While planar thermoelectric textiles address certain limitations of linear thermoelectric textiles, they still reflect the inherent trade-offs between organic and inorganic thermoelectric materials. Organic conductive polymers, though flexible and compatible with textiles, typically exhibit lower Seebeck coefficients compared to inorganic materials. In contrast, inorganic materials excel in thermoelectric performance but suffer from brittleness, poor flexibility, and integration challenges. Therefore, hybrid approaches, combining organic polymers with inorganic materials, offer a pathway to enhance performance while maintaining flexibility and scalability.

4 Used methods, study material

4.1 Materials

The Cu-coated nonwoven fabric, commercially known as MEFTEX 20 (M20), was purchased from Bochemie a.s. (Czech Republic) and is intended to serve as the substrate for electroplating. MEFTEX 20 has an average areal density of 25 ± 1 g/m² and a thickness of 0.074 ± 0.05 mm. MEFTEX 20 is composed of a 20 g/m² polyethylene terephthalate (PET) nonwoven fabric (MILIFE 20) manufactured by ENEOS Techno Materials Corporation (Japan), and an additional Cu deposition layer with an areal density of 5 g/m², as shown in Figure 4.1(A). The preparation process of MEFTEX 20, involving chemical Cu deposition followed by electroplating. MILIFE 20 is a 100% polyester (PET) nonwoven fabric composed of continuous polyester filaments with an approximate diameter of 10 µm. The nonwoven fabric is created with one layer in the machine direction and the other in the cross direction connected by thermal bonding. To investigate the influence of MEFTEX 20's structure on its thermoelectric properties, a sample prepared solely through chemical Cu deposition was also purchased and designated as Cu-PET-CD.

The chemicals are used for Ni electroplating on MEFTEX 20 fabric, including nickel sulfate ($NiSO_4 \cdot 6H_2O$), nickel chloride ($NiCl_2 \cdot 6H_2O$), boric acid (H_3BO_3) and sulfuric acid (H_2SO_4). All the chemicals were purchased from Sigma Aldrich (USA).

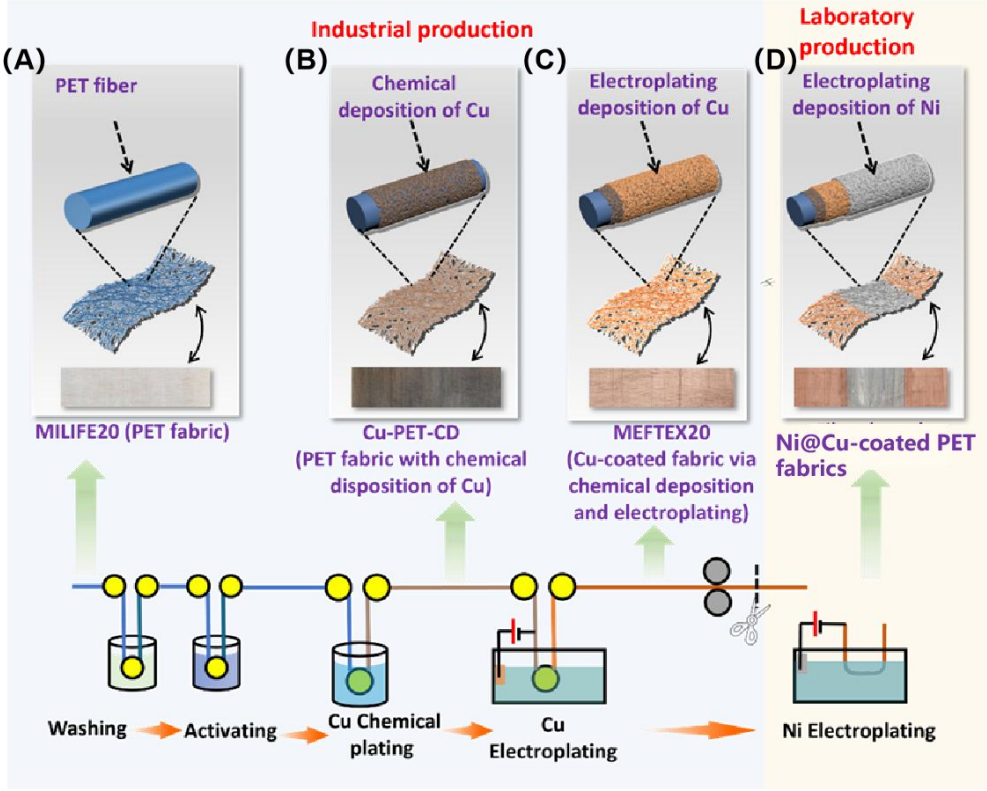

Figure 4.1 Prepartation of Ni@Cu-coated PET fabrics with TE property (A: diagram of MILIFE20, B: diagram of MEFTEX20, C: diagram of Cu-PET-CD, and D: diagram of Ni@Cu-coated PET fabrics

4.2 Sample preparation

The sample was prepared by partially depositing Ni on the M20 via electroplating. The details are as follows:

- Sample preparation

The M20 fabric was first cut into a tape with 60 cm length and 5 cm width. Then, the central segment with 20 cm length of M20 was marked for following Ni deposition via electroplating.

- Pretreatment

To eliminate impurities such as grease and fats, the M20 sample was immersed in a 10% H_2SO_4 solution for 15 seconds. This was followed by a thorough rinse with deionized water for 1 minute to ensure the complete removal of residual acid and contaminants.

- Preparation of Watt nickel (Ni) bath

The Watt Ni bath was formulated by dissolving 51 g of $NiSO_4 \cdot 6H_2O$, 110 g of $NiCl_2 \cdot 6H_2O$, and 6 g of H_3BO_3 into 300 g of deionized water (DW) with continuous stirring until a uniform solution was obtained.

- Ni Electroplating setup and sample preparation

A custom system was developed for Ni electroplating on the central 20 cm segment of the MEFTEX20 sample (M20). This system included a DC power supply (0–5 V, 0–1 A), two nickel (Ni) plates, and a container. The prepared Watt Ni bath was added to the PP container, and the central segment of M20 was fully submerged in the solution. The ends of the M20 sample were connected to the negative terminal of the DC power supply, while the Ni plates were attached to the positive terminal.

The electroplating process was carried out at 19°C and 55% relative humidity, with a controlled current density of 0.02 A/cm². Ni deposition was performed for 6, 8, 10, and 20 minutes, resulting in four Ni@Cu-coated PET fabric samples.

Each sample consisted of three sections: a Cu-coated PET fabric（M20）(part 1), a Ni@Cu-coated PET fabric (part 2), and another Cu-coated PET fabric（M20）(part 3). These samples were labeled as sample-t, where "t" represents the electroplating duration. For example, Ni@Cu-coated PET fabric sample-6min corresponds to the sample electroplated for 6 minutes, which can be abbreviated as Ni@M20-6min.

The Ni-deposited region (Ni@Cu-coated PET fabric) was labeled as Ni@M20-t, with "t" indicating the electroplating time. For instance, Ni@M20-6min refers to the Ni@Cu-coated PET fabric electroplated for 6 minutes. Additionally, in our initial experimental studies, it was observed that nickel electroplating on copper foil using the same method resulted in low thermoelectric performance. To investigate this issue and identify the underlying reasons, a comparative study was conducted. Copper foil, nickel-plated copper foil, and other samples were electroplated under identical methods and conditions.

- Ni@Cu-coated PET fabric with different widths

To investigate the influence of width on the thermoelectric (TE) properties of fiber-based Ni@M20 samples, the prepared Ni@M20-t samples were cut into smaller samples with varying widths. The widths were set to 1 cm, 1.5 cm, 2 cm, and 5 cm. These fiber-based Ni@M20 samples with different widths were labeled as Ni@M20-t-w. For instance, a sample labeled as Ni@M20-6min-1cm refers to a Ni@Cu-coated PET fabric sample prepared with 6 minutes of Ni electroplating and a width of 1 cm.

4.3 Characterizations

4.3.1 Characterization of morphology

The morphology of Ni@Cu-coated PET fabrics was characterized using scanning electron microscopy (SEM) combined with focused ion beam (FIB) and energy-dispersive X-ray spectroscopy (EDX) at an operating voltage of 20 kV. To analyze the surface porosity from SEM images in software ImageJ, the image is first imported, and the threshold is adjusted (threshold = 30) to distinguish pore areas from solid regions. The Analyze Particles tool is then used to calculate the pore area as a percentage of the total surface area, providing a measure of porosity. Additionally, FIB-SEM was employed to characterize the elemental composition of the sample.

4.3.2 Characterization of crystalline structure

The crystalline structure of Cu, Ni, and potential metal oxides in the samples was characterized using an X-ray diffractometer (XRD) (X'pert PRO, PANalytical, Netherlands) with a Cu Kα radiation source (λ = 1.54 Å). The operating voltage and current were set at 40 kV and 40 mA, respectively. Additionally, focused ion beam-transmission electron microscopy (FIB-TEM) was employed to examine the crystalline structure of the Ni and Cu coating layers. The lattice distances estimated from FIB-TEM were compared with standard lattice distances of Ni and Cu-based materials to identify and confirm the components. The grain size and D-space distance of Ni crystal and Cu crystal of Ni@Cu-coated PET fabric according to Equation 4.1 and 4.2

$$\delta = \frac{K\lambda}{FWHM \cdot \cos\theta} \tag{4.1}$$

$$d = \frac{q\lambda}{2\sin\theta} \tag{4.2}$$

The δ is the grain size (nm) d is the D-spacing distance (Å), q is the diffraction order, λ is the wavelength (nm), θ is the diffraction angle (°), K is constant of 0.9, and $FWHM$ is the width at half height of the peak (°).

4.3.3 Characterization of element valence

The chemical valence of Ni@Cu-coated PET fabrics and potential metal oxides was analyzed using X-ray photoelectron spectroscopy (XPS) with an Al Kα X-ray source. A full survey scan was conducted to identify all elements present on the surface, including C, O, Ni, and Cu. High-resolution scans were then performed for Ni 2p, Cu 2p, O 1s, and C 1s to determine the chemical states and oxidation levels of the elements.

4.3.4 Characterization of electrical conductivity

The electrical conductivity of Ni@Cu-coated PET fabrics was evaluated in accordance with the standard ASTM D257-14 under controlled room conditions, with a temperature of 23 ± 1 °C and relative humidity of 55 ± 1%. As the Equation (4.3) and (4.4) show, both surface resistivity $p_S(\Omega)$ and volume resistivity p_v (Ω·m) were measured using an Agilent 5313A resistance meter equipped with a circular electrode. To ensure statistical reliability, each sample was measured five times.

$$p_{S=}R_{S\cdot}\frac{o}{l} \tag{4.3}$$

$$p_{v=}R_{v\cdot}\frac{s}{h} \tag{4.4}$$

Where $R_{S\cdot}$ is the surface resistance (Ω), o is the middle perimeter of electrodes (m), l is the distance between electrodes (m). R_v is the volume resistance (Ω·m), S is the area of electrodes (m), h is the thickness of samples (m).

4.3.5 Characterization of thermal conductivity and thermal resistance

The ALAMBETA device was used to measure the thermal conductivity K ($W \cdot m^{-1} \cdot K^{-1}$) and thermal resistance R_t ($m^2 \cdot K \cdot W^{-1}$) of the Ni@Cu-coated PET fabric in accordance with Standard EN 31092. The measurements were conducted at a temperature of 25 ± 1 °C and a relative humidity of 65 ± 1%.

During testing, the device applied a pressure of 200 Pa, ensuring stable thermal interaction between the sample and the sensor head. The thermal resistance R_t ($m^2 \cdot K \cdot W^{-1}$), defined as the ratio of sample thickness (mm) to its thermal conductivity ($W \cdot m^{-1} \cdot K^{-1}$), was also evaluated. Given the variations in thickness, the results include both thickness (mm) and thermal resistance at 200 Pa for accurate comparison. Each sample was tested five times to ensure statistical accuracy.

4.3.6 Characterization of EMI shielding

The electromagnetic interference (EMI) shielding performance of the Ni@Cu-coated PET fabric was evaluated using the coaxial transmission line method, following the ASTM D4935-10 standard as described in [36]. Tests were conducted under controlled room conditions, maintaining a temperature of 25 ± 1 °C and a relative humidity of 65 ± 1%. Each sample was measured five times to ensure statistical reliability.

According to the ASTM D4935-10 standard, the method assumes the impact of a plane wave on a shielding material at frequencies ranging from 30 MHz to 3 GHz. The measurement setup consisted of a coaxial specimen holder (Electro-Metrics, Inc., EM-2107A) and a vector network analyzer (Rohde & Schwarz ZNC3). The input and output signals were connected to the analyzer, and the shielding effectiveness (SE) was calculated using the forward transmission coefficient SE_T. Specifically, P_T and $P_I$refer to the transmittance power and incident power, respectively.

$$SE_T = -10 \log P \frac{P_T}{P_I} \tag{4.5}$$

4.3.7 Characterization of air permeability

The air permeability of the Ni@Cu-coated PET fabrics was evaluated using an FX 3300 standard air permeability tester (TESTEX AG, Switzerland) according to the ISO 9237 standard. The tests were conducted under controlled room conditions, with a temperature of 25 ± 1 °C and relative humidity of 65 ± 1%. Air permeability measurements were performed at two pressure difference

values, 100 Pa and 200 Pa, using a circular test clamp with a measurement area of 20 cm^2. Each sample was tested five times and the results averaged.

4.3.8 Characterization of TE behavior

The thermoelectric behavior of Ni@Cu-coated PET fabrics was characterized using two custom setups designed for a continuous cooling model and a controlled temperature model, respectively, which will be explained in the next subsections. The controlled temperature model adheres to standard practices, where thermoelectric behavior is measured by maintaining specific hot-end and cold-end temperatures. In this process, the temperature gradient drives the diffusion of charge carriers, leading to a potential difference. This phenomenon underpins the Seebeck effect in thermoelectric materials.

4.3.8.1 TE behavior measured via controlled temperature difference model

As shown in Figure 4.2, a controlled temperature model was employed to validate the stability of thermoelectric behavior measured using a controlled temperature difference model. Prior to measurement, the surface of a plate heater was heated to a fixed temperature and stabilized. A Ni/Cu boundary (the boundary between Part 1 and Part 2, labeled as the hot end) was placed on the surface of the plate heater. The other Ni/Cu boundary (the boundary between Part 2 and Part 3, labeled as the cold end) was positioned on the surface of a temperature-controlled insulated material.
To record the temperatures at both ends, K-type thermocouples connected to a temperature multimeter (Voltcraft, Germany) were tightly attached to each end. Simultaneously, another set of K-type wires connected to a digital multimeter (DMM 6500, Keithley) was attached to the outer Cu coating part to measure the voltage. After a stabilization period of one minute, the temperatures at both ends and the voltage output were recorded.
To minimize potential interference from heat conduction across the sample surface or temperature fluctuations in other areas, the temperature was maintained at relatively low levels. The temperature difference was controlled between 14 ℃ and 62 ℃, with intervals of 5 ℃. At each temperature difference, the voltage output was measured three times. For statistical analysis of the thermoelectric behavior, the measurements for each sample were repeated five times.

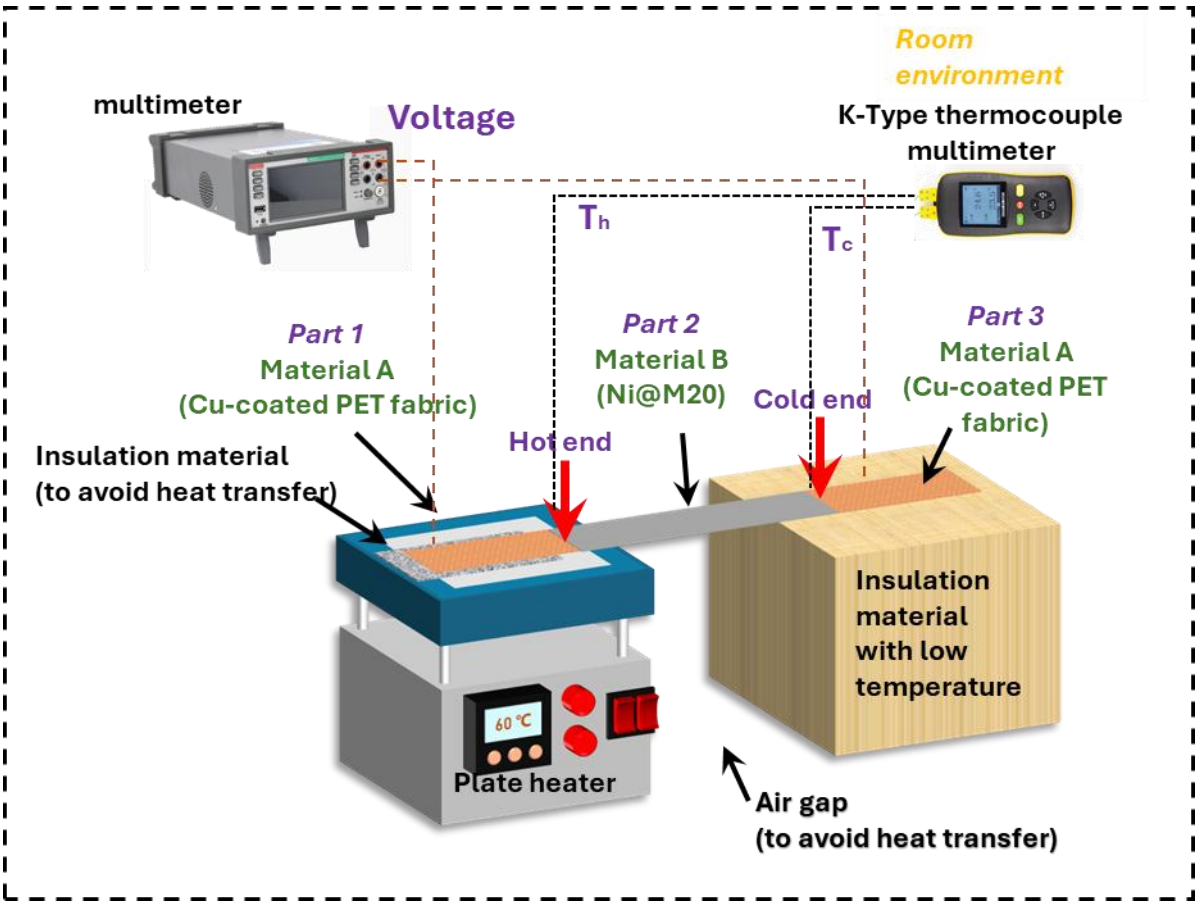

Figure 4.2 Thermoelectrical measurement with controlled hot end at controlled temperature

4.3.8.2 TE behavior measured via continuous cooling model

As shown in Figure 4.3, the sample's thermoelectric behavior was evaluated using a continuous cooling model. Similarly, one Ni/Cu boundary (the boundary between Part 1 and Part 2, labeled as the hot end) was inserted into the rod heater. The other Ni/Cu boundary (the boundary between Part 2 and Part 3, labeled as the cold end) was positioned on the surface of a temperature-controlled insulated material.

Thermocouple with two wires connected to a temperature multimeter (Voltcraft, Germany) were closely attached to both ends of the sample to record the temperatures. Simultaneously, another pair of K-type wires connected to a voltage multimeter (DMM 6500, Keithley Multimeter) contacted the outer Cu coating layers to measure the voltage. During the measurement, the rod heater was heated to 120 °C. Subsequently, the power was switched off to initiate the cooling process, and the thermoelectric behavior was recorded by monitoring the temperatures at both ends, the voltage output, and the elapsed time. Each sample was tested five times to obtain statistical data on thermoelectric behavior.

To address potential factors affecting thermoelectric behavior, we investigated sample deformation and fluctuations. Fluctuations caused by wind, which may result from environmental factors such as movement, were evaluated by simulating a wind speed of 2 m/s. This wind speed corresponds to the typical speed observed during ordinary walking. The thermoelectric behavior of the sample under fluctuating and non-fluctuating conditions was compared to analyze the impact of wind on its performance.

In addition, the effect of sample deformation was studied. The sample was twisted by fixing both the hot and cold ends. The continuous cooling model was then applied to the twisted sample, and the resulting thermoelectric behavior was compared with that of the untwisted sample to evaluate the impact of twisting deformation on thermoelectric performance.

To investigate the effects of water washing on thermoelectric performance and material stability, the experimental method was refined following standard ISO 105-C06 textile washing procedures. The samples showed the best thermoelectric performance, was selected for testing. The sample was washed at 40°C for 30 minutes using 1 g/L of detergent, followed by drying.

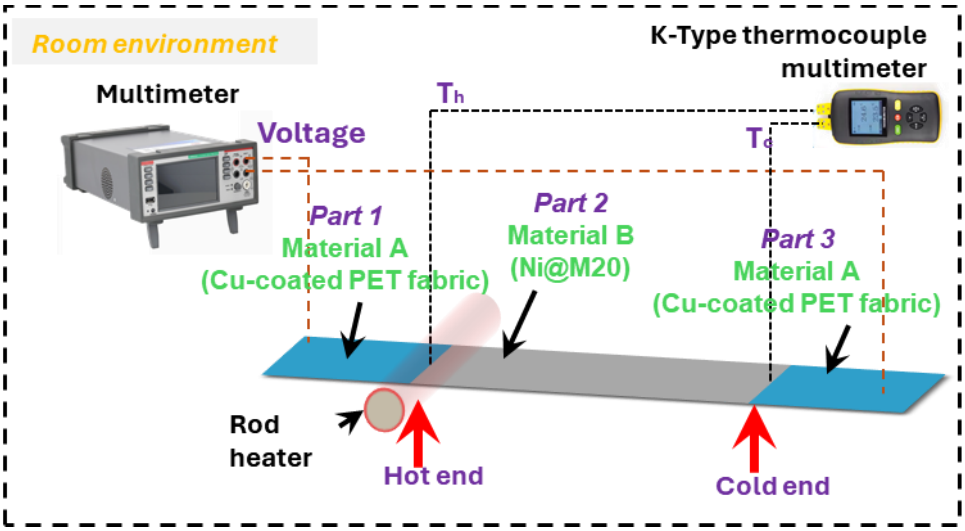

Figure 4.3 Thermoelectrical measurement with continuous cooling model

5 Summary of the results achieved

5.1 Structural analysis of Ni@Cu-coated PET fabrics

5.1.1 Morphology characterization of Ni@Cu-coated PET fabrics

The morphology of Cu-coated PET fabric (M20) and Ni@M20 fabrics are shown in Figure 5.1. After electroplating, the Ni is well deposited on Cu layer:

- Early stage of Ni plating (6 minutes): Ni ions preferentially form nuclei on the surface of the copper substrate and these nuclei gradually grow into small particles. Due to the good interfacial bonding between copper and nickel, the Ni particles are evenly distributed on the copper surface.
- Intermediate stage (8–10 minutes): As plating time increases, Ni ions continue to deposit onto existing particles, resulting in their enlargement and coarsening. Uneven grain growth begins to emerge, primarily caused by the merging of neighboring particles (grain enlargement) or the continued deposition of nickel atoms onto the same particles.
- Prolonged plating (20 minutes): The Ni particles were observed to become highly compact and fine-grained, as expected. This outcome is attributed to the presence of nickel chloride ($NiCl_2$) in the plating solution, which promotes nucleation, inhibits grain growth, and enhances deposition uniformity, effectively refining the grain structure of the nickel layer. Additionally, the use of low current densities (0.02 A/cm²) further contributes to this process by allowing for more homogeneous deposition of Ni ions, thereby supporting the formation of fine grains.

However, minor surface defects, such as holes, were observed on both the Cu-coated PET fabric (M20) and the Ni@Cu-coated PET fabric (Ni@M20-t). Some of these holes are attributed to insufficient copper deposition on the PET fibers during the preparation of the M20.

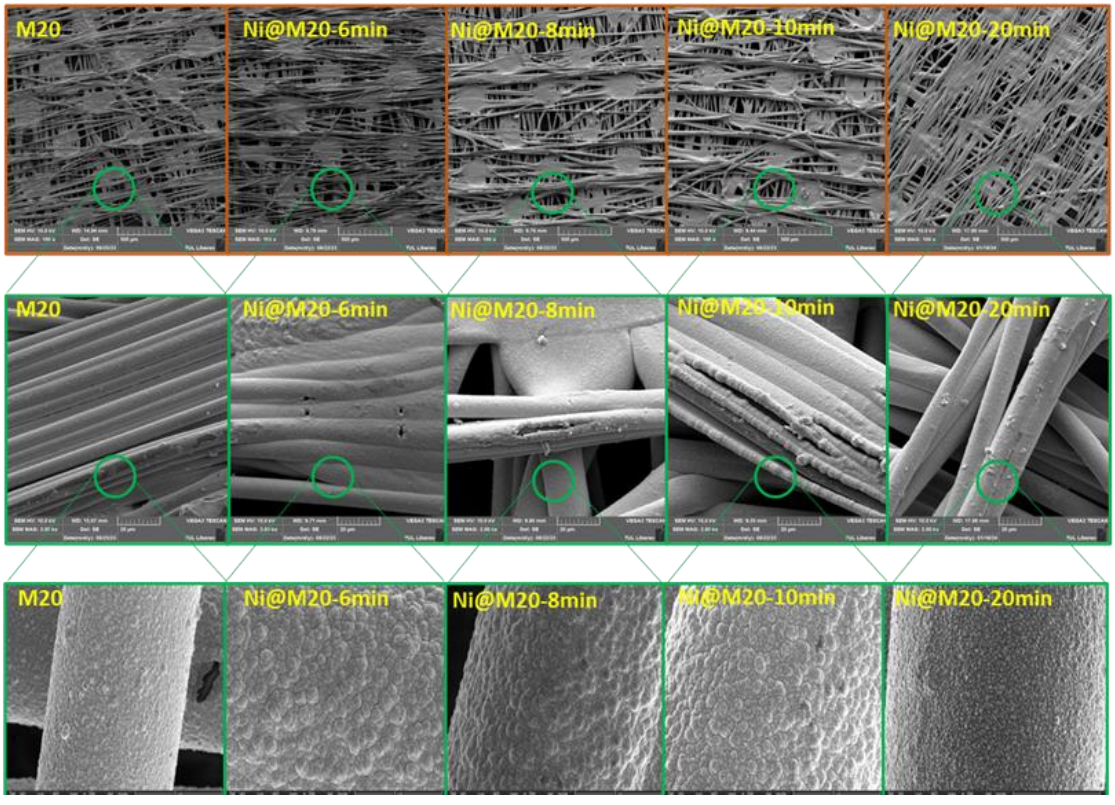

Figure 5.1 Morphology of Cu-coated fabric MEFTEX20 (M20) and Ni@Cu-coated PET fabric

(Ni@M20-t).

5.1.2 Surface porosity analysis of Ni@Cu-coated PET fabrics

With increased coating time (t), the amount of Ni deposited on the surface increases, and the ratio of nickel to copper ($R_{Ni/Cu}$) exhibits a linear relationship with t, as shown in Figure 5.2 (A). Concurrently, the surface porosity decreases following a linear decreasing trend, as illustrated in Figure 5.2 (B). This reduction in porosity is due to the progressive coverage of Ni particles on the Cu-coated fibers, which effectively reduces voids and enhances the uniformity of the coating

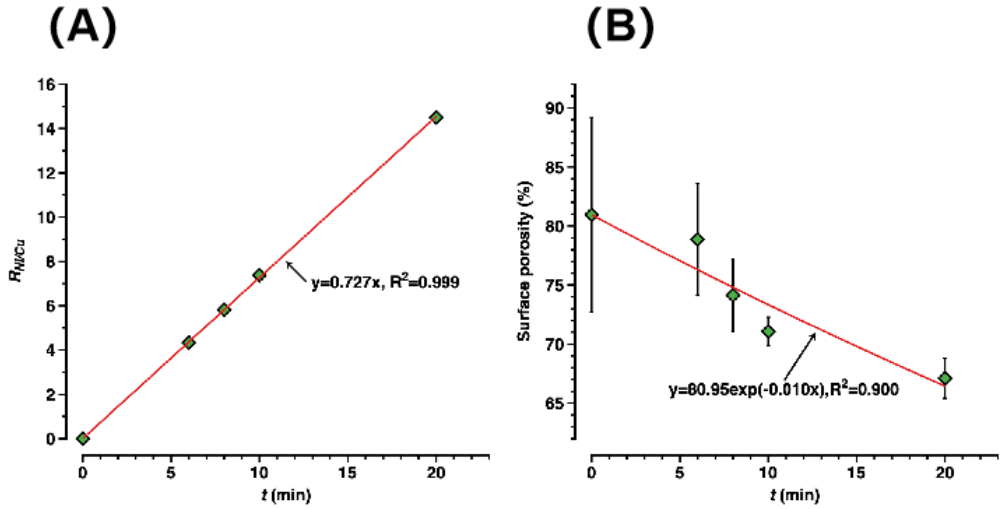

Figure 5.2 Change of $R_{Ni/Cu}$ (A) and surface porosity (B) with time t

5.1.3 Cross-section morphology analysis of Ni deposition layer

To further investigate the morphology, a cross-sectional sample of the Ni@Cu-coated fabric was prepared for elemental analysis, as illustrated in Figure 5.3 (A). All Ni@M20 fabrics share a similar structure, consisting of a Ni coating layer, a Cu coating layer, and PET fibers. To illustrate these features, the Ni@M20-8min sample was selected as a representative example. As revealed by the FIB-SEM-EDX analysis in Figure 5.3(B), the Ni deposition layer, Cu deposition layer, and PET fibers are distinctly observed, providing a clear visualization of the structural composition.
The Ni coating layer has a thickness of 356±108 nm, while the Cu coating layer measures 326±14 nm, with both layers at the nanoscale. As described in section 4.1‘Materials', the Cu-coated fabric (M20) features two distinct Cu deposition layers due to its preparation process: the chemical Cu deposition layer, forming the bottom layer, and the electroplating Cu deposition layer, forming the upper layer. To distinguish between these two layers, six points from the upper and bottom layers of the Cu coating were analyzed using EDX, as shown in Figure 5.3 (C). The results, exemplified by points 2 and 5 from the Ni@Cu-8min sample in Figure 5.3 (D), reveal distinct compositional differences. The bottom layer contains approximately 13% oxygen (O) and 87% copper (Cu), indicating a significant presence of copper oxides. In contrast, the upper layer consists of about 0.5% oxygen (O) and 99.5% copper (Cu), signifying nearly pure copper. These findings confirm that the chemical copper deposition layer contains more copper oxides, whereas the electroplated copper deposition layer is predominantly pure copper. As a result, copper oxides are an inherent feature of all Ni@Cu-coated PET fabrics.

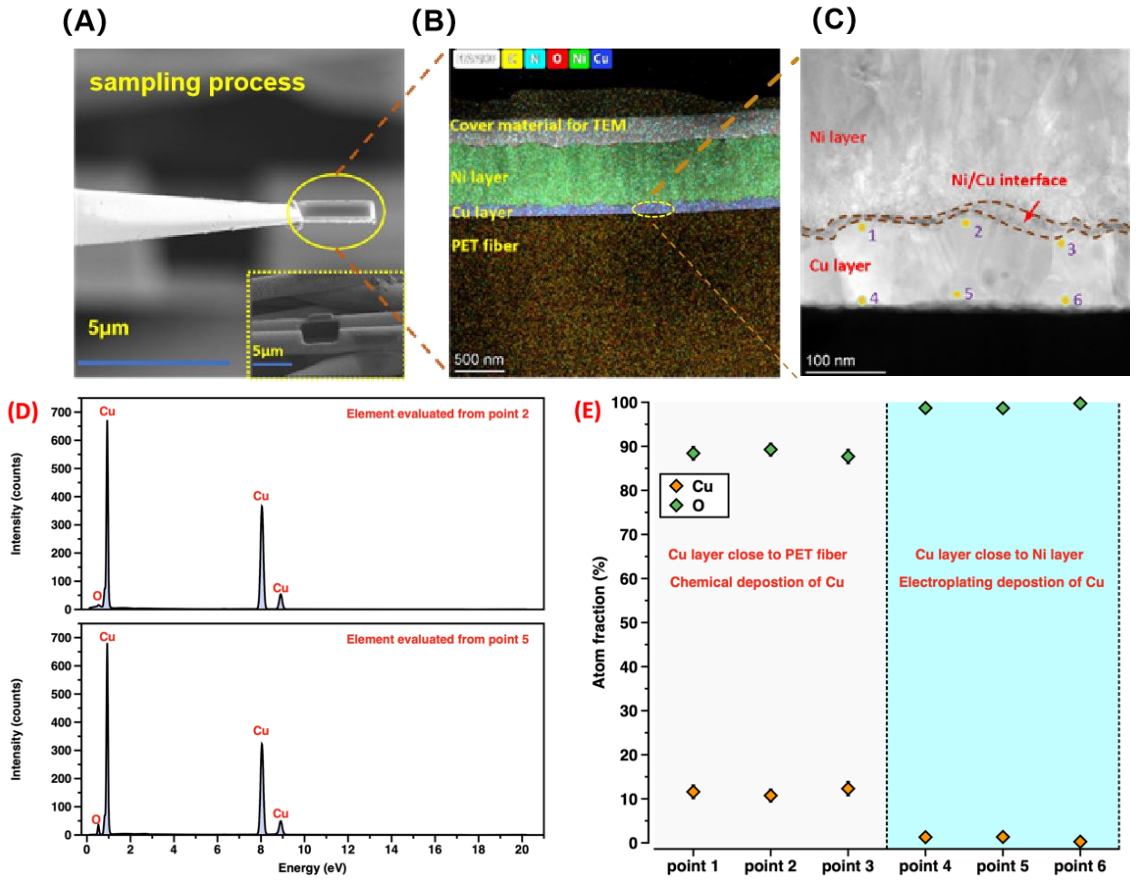

Figure 5.3 FIB-SEM-EDX analysis of sample Ni@M20-8min (A: Cross-section sampling, B: EDX, C: SEM with large magnification, D: two examples for element analysis, and E: Cu and O atom fraction of measured points)

5.2 Crystalline structure analysis of Ni@Cu-coated PET fabrics

To gain deeper insights into the crystalline characteristics and structural details of Ni and Cu within the Ni@Cu-coated PET fabrics, XRD peak fitting was conducted using the Gaussian method. As shown in Figure 5.4, for Cu and Ni, two planes are identified: [111] and [200]. Table 5.1 provides calculated grain size and D-space distance of Ni crystal and Cu crystal of Ni@Cu-coated PET fabric.

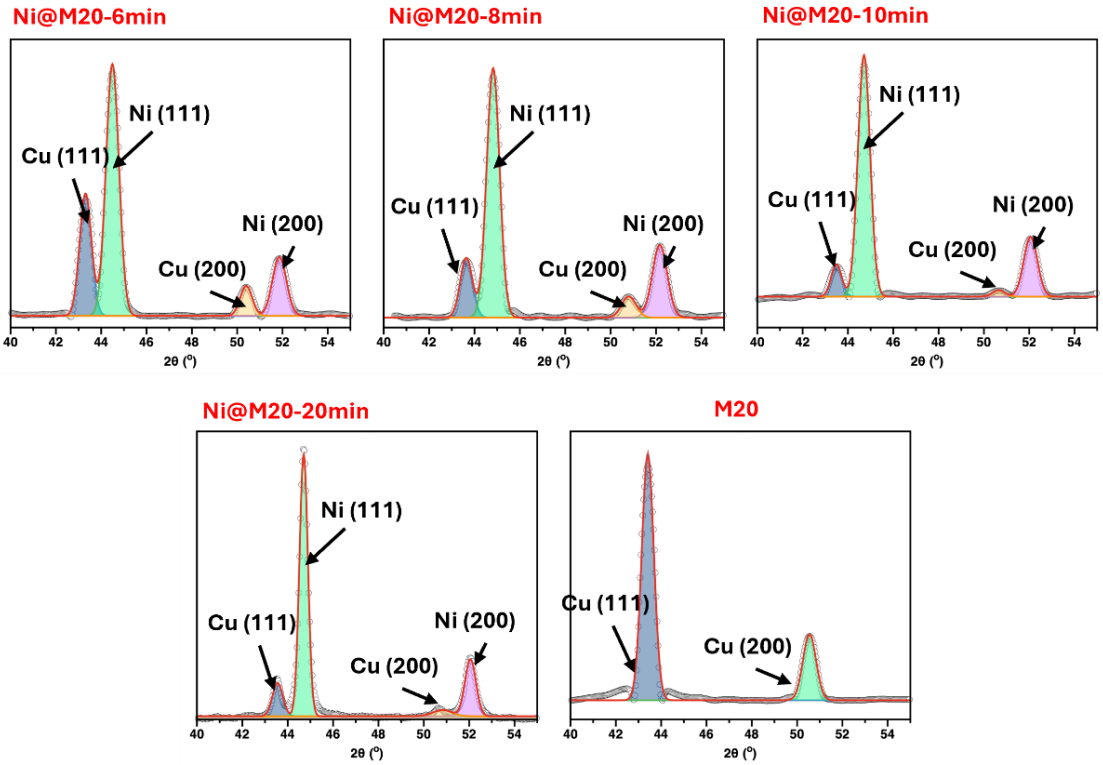

Figure 5.4 Gaussian fitting for Ni and Cu crystalline structure of Ni@Cu-coated PET

Table 5.1 Crystalline structure of Ni and Cu of prepared samples

Label	Cu (111) at ~44°		Cu (200) at ~50°		Ni (111) at ~44.50°		Ni (200) at ~52°	
	δ (nm)	d (Å)	δ (nm)	d (Å)	δ (nm)	d (Å)	δ (nm)	d (Å)
M20	13.617	1.120	12.902	0.998	-	-	-	-
Ni@M20-6min	13.844	1.123	12.057	0.999	12.762	1.098	14.284	0.979
Ni@M20-8min	13.511	1.115	11.376	0.994	12.796	1.092	11.943	0.974
Ni@M20-10min	13.519	1.117	16.184	0.996	12.076	1.096	13.713	0.977
Ni@M20-20min	13.518	1.117	16.187	0.995	12.078	1.095	13.715	0.976

Building on this analysis, a comprehensive summary of the XRD results is presented in Figure 5.5, providing an overarching view of the crystalline structures and their key characteristics. PET fibers exhibit three crystalline planes: [110], [002], and [101] Interestingly, Cu oxides are not observed in the XRD results, likely due to the limited penetration depth of this technique. To further understand the M20 and Ni@M20 samples, the chemical Cu-coated PET fabric sample (Cu-PET-CD) was also examined, in addition to the PET crystalline structure, both Cu and Cu_2O were detected. Specifically, Cu_2O shows two planes, [111] and [200], while Cu is characterized by a single plane, [111].

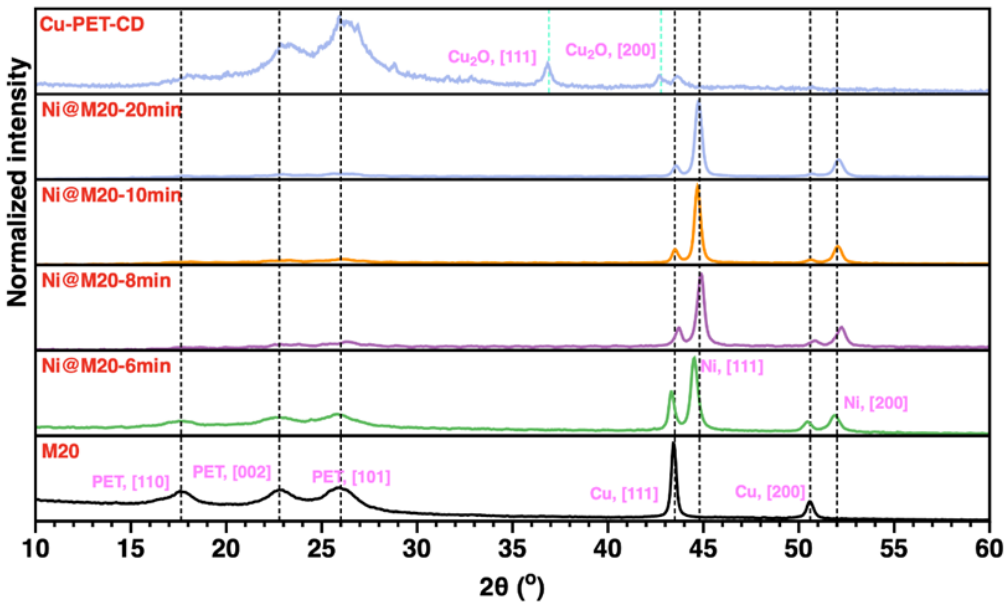

Figure 5.5 XRD curve of all the samples

5.3 Chemical valence analysis of Ni@Cu-coated PET fabrics

To further confirm the structure of the Cu oxides, the element and valence of the sample were revealed via XPS. The XPS results and corresponding peak fittings for samples Cu-PET-CD, M20, Ni@M20-6min, and Ni@M20-20min are shown in Figures 5.6, 5.7, 5.8, and 5.9 respectively. It is noticed XPS is the technology focusing on surface. The Cu2p scan is unclear when there is the Ni deposition, which is proven from Cu2p scan of Ni@M20-6min and Ni@M20-20 min. Therefore, only the Cu2p scan of M20 is conducted. Additionally, Ni2p scan of Ni@M20-6min and Ni@M20-20 min were performed to reveal the effect of coating time on the Ni element valence. Elemental analysis based on the Cu2p, O1s, and Ni2p scans for all samples is summarized in Tables 5.2, 5.3, and 5.4. The identification of elemental valence states is conducted in accordance with the XPS database (The International XPS Database of Monochromatic XPS Reference Spectra).

- For Cu-PET-CD and M20 sample

As shown in Figure 5.6, the full survey scan from the XPS analysis reveals the presence of Cu, C, and O elements of sample Cu-coated PET fabric with only chemical deposition (Cu-PET-CD) are detected. The element valences of XPS scans for Cu2p and O1s are listed in Table 5.2 and Table 5.3 respectively. The Cu2p scan of the sample Cu-PET-CD is presented in Figure 5.6. The presence of Cu^{2+} is clearly confirmed by the satellite peak near 962 eV, along with additional satellite peaks in the range of 940-945 eV. In the binding energy range from 932-935 eV, two peaks are observed, corresponding to three species: Cu^{1+} from Cu_2O at 932.5 eV, Cu^{2+} from CuO at 933 eV, and Cu^{2+} from Cu $(OH)_2$ at 934.4 eV. This indicates that Cu native oxides are found in the Cu-PET-CD. Besides, the peak as satellite at about 944 eV corresponding to Cu is found. Therefore, Cu element is also found in Cu-PET-CD. The sample M20 exhibits a similar Cu valence state to sample Cu-PET-CD, confirming the presence of native Cu oxides in M20. As shown in Figures 5.7, the only one difference is the peak at 933 eV contributed from Cu^{2+} (CuO) disappears, and peak at 940 eV contributed from Cu^{2+} (CuO) is weaken. It suggests that electroplating process reduces the presence

of CuO. By combining with FIB-SEM-EDX, the Cu-based element in Ni@Cu-coated PET fabrics includes crystalline Cu, crystalline Cu_2O amorphous CuO, and the amorphous $Cu(OH)_2$.

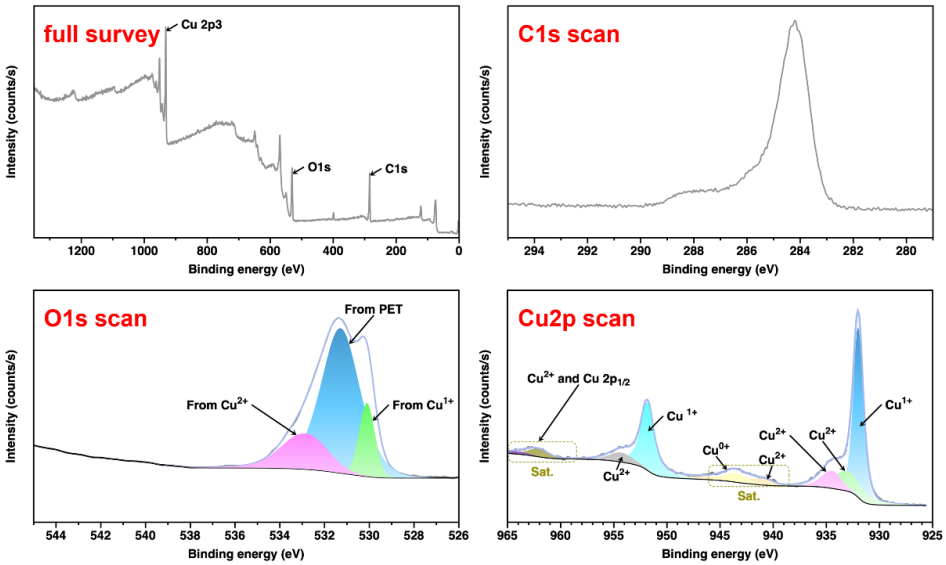

Figure 5.6 XPS results of sample Cu-PET-CD

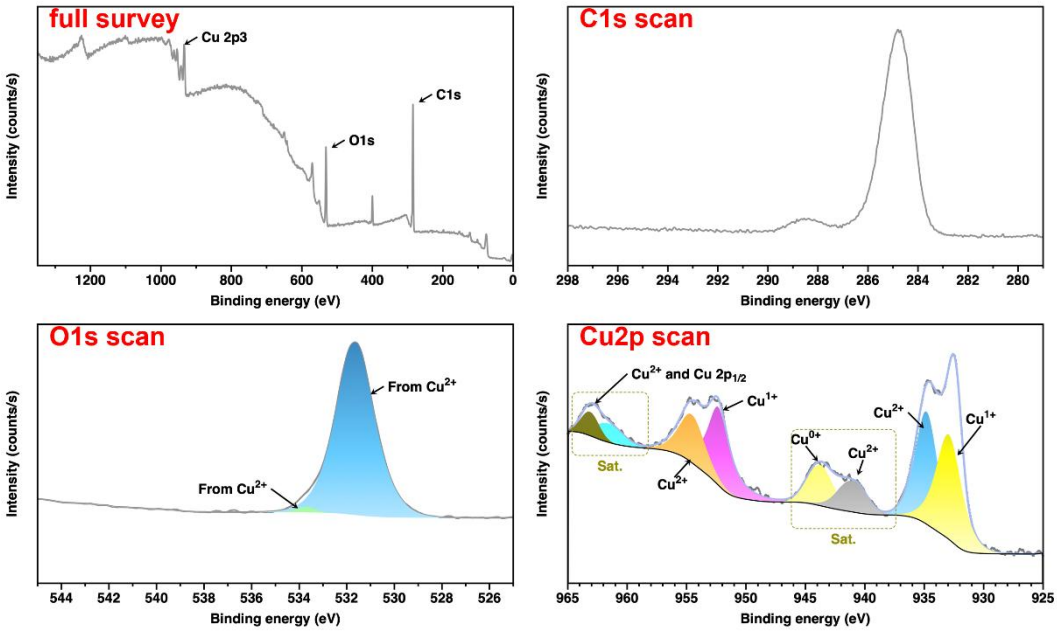

Figure 5.7 XPS results of sample M20

- For sample Ni@M20-6min

The full XPS survey of sample Ni@M20-6min is shown in Figure 5.8, and Ni element, Cu element, C element and O element are detected. The presence of Ni^{2+} is found from Ni2p scan, and correspondingly O^{2-} related to Ni^{2+} is found. Therefore, NiO exists in Ni@M20-6min. It could be caused by surface oxidation. However, the low resistance observed (as will be detailed in Section 5.4) indicates that the amount of Ni oxides is minimal.

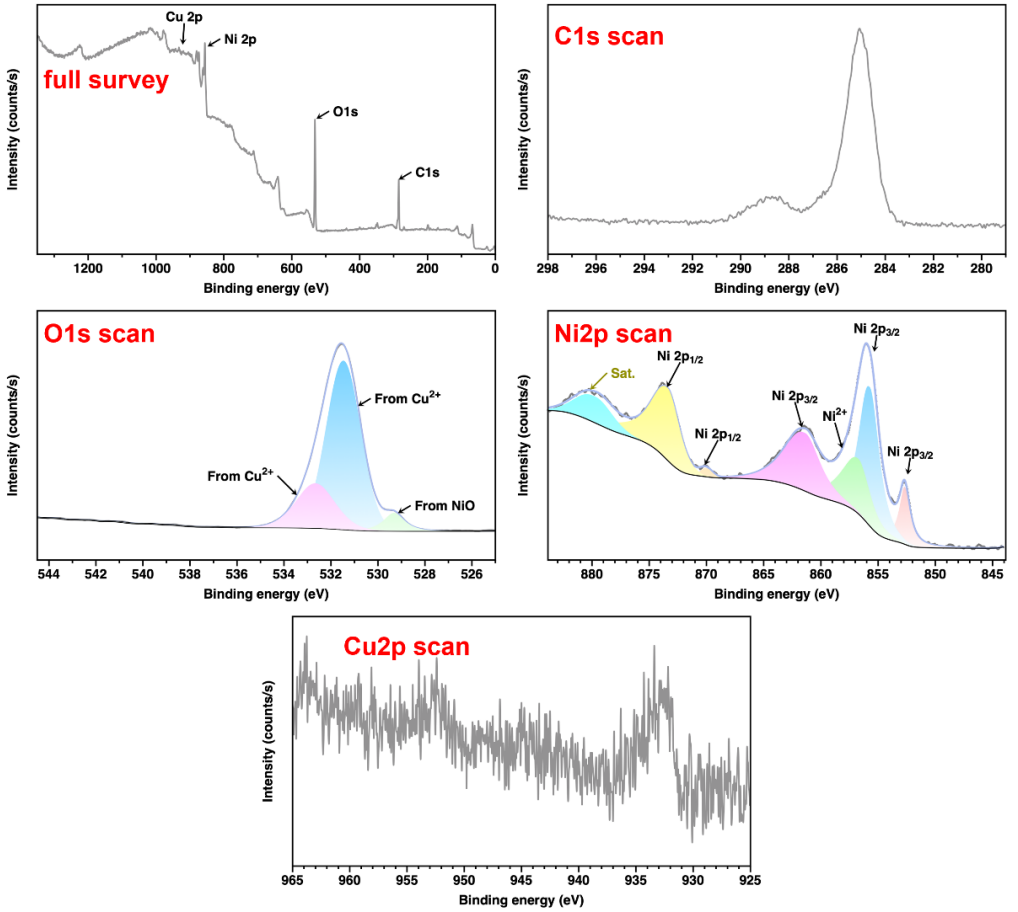

Figure 5.8 XPS results of Ni@M20-6min

- For sample Ni@M20-20min

Figure 5.9 presents the full XPS survey and Ni2p scan of sample Ni@M20-20min. By comparing with sample Ni@M20-6min, all the elements are similar. Consequently, coating time does not affect the Ni element valence.

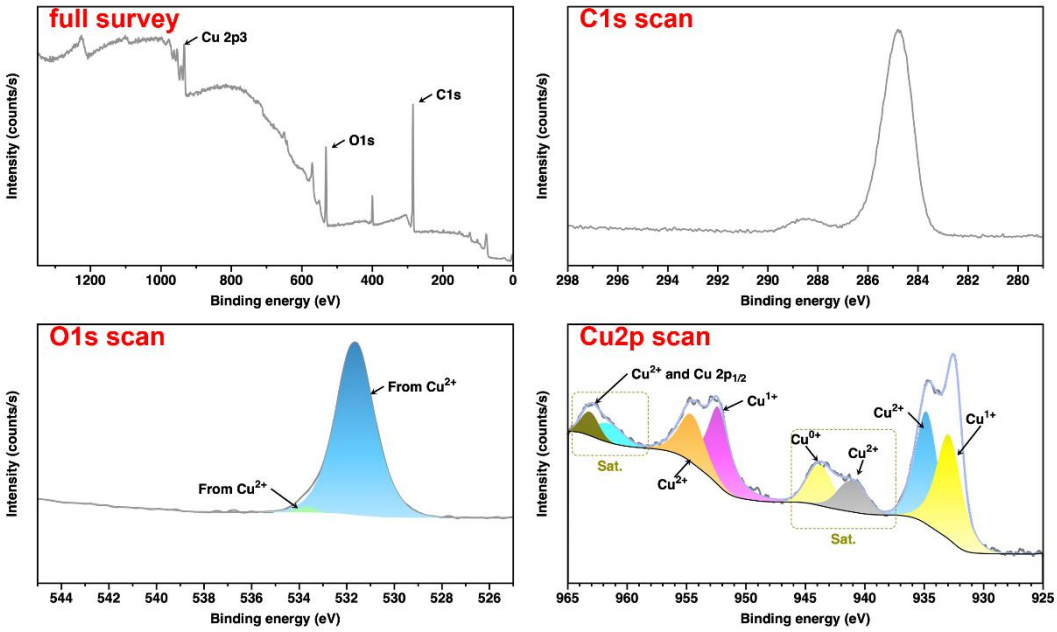

Figure 5.9 XPS results of Ni@M20-20min

Table 5.2 Element valence according to Cu2p scan from XPS analysis

Binding energy (eV)	Valence
932.5	Cu^{1+} (Cu_2O)
933	Cu^{2+}(CuO)
934.4	Cu^{2+}(Cu $(OH)_2$)
940.9	Cu^{2+}(CuO) (Sat.)
943.52	Cu^{0+}(Cu) (Sat.)
951.82	Cu^{1+}(Cu_2O)
954.34	Cu^{0+}(Cu)
962 963.43	Cu^{2+} and Cu^{0+} (Sat.)

Table 5.3 Element valence according to O1s scan from XPS analysis

Binding energy (eV)	Valence
529.5	O^{2-} with combination of Ni^{2+}
530.5	O^{2-} with combination of Cu^{1+}
531.5	O^{2-} from PET
533.7	O^{2-} with combination of Cu^{2+}

Table 5.4 Element valence according to Ni2p scan from XPS analysis

Binding energy (eV)	Valence
852.7	Ni $2p_{3/2}$
856.1	Ni $2p_{3/2}$
857.0	Ni^{2+}
861.5	Ni $2p_{3/2}$
870.1	Ni $2p_{1/2}$
873.8	Ni $2p_{1/2}$
880.3	Sat.

5.4 Effect of Ni deposition on electrical conductivity property and EMI shielding

5.4.1 Effect of Ni deposition on electrical conductivity

Figure 5.10 (A) and (B) illustrate the volume resistivity and surface resistivity of Ni@Cu-coated PET fabrics with varying $R_{Ni/Cu}$ values, reflecting the impact of nickel content on the electrical properties of the material. As the $R_{Ni/Cu}$ value increases, both volume resistivity and surface resistivity decrease, indicating an improvement in electrical conductivity. Specifically, the volume resistivity decreases from 34.3 Ω·m to 9.95 Ω·m, while the surface resistivity decreases from 1.37 Ω to 1.13 Ω. This trend suggests that higher nickel deposition enhances conductivity by forming a more continuous conductive layer, improving charge transport despite nickel's lower conductivity than copper.

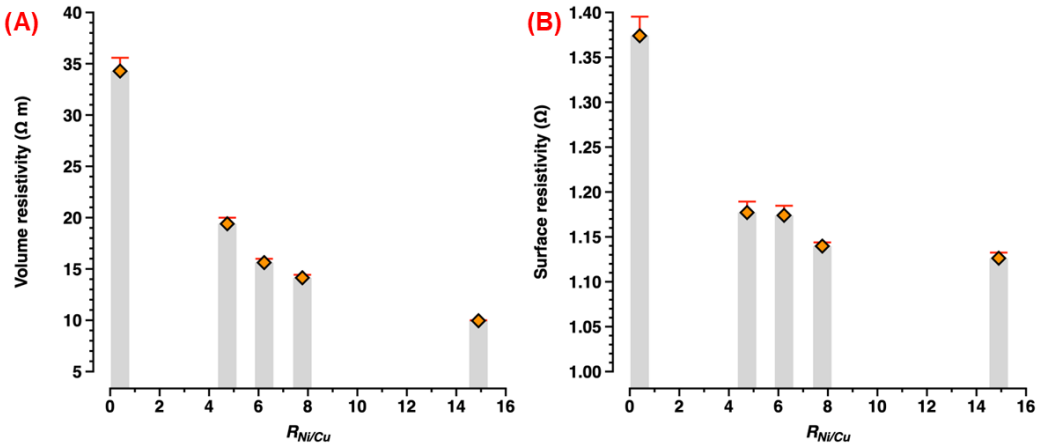

Figure 5.10 (A) volume resistivity (B) surface resistivity of Ni@M20 samples

5.4.2 Effect of Ni deposition on EMI shielding

Conductivity is a fundamental factor in electromagnetic interference (EMI) shielding, and maintaining high conductivity is crucial for achieving effective shielding performance. Although the overall conductivity decreases slightly with increasing nickel content compared to copper, the Ni@Cu-coated PET fabrics still exhibit excellent electrical conductivity, which is central to their strong EMI shielding capabilities.

Due to their low electrical resistivity, the Ni@M20 samples exhibit effective EMI shielding performance, See Table 5.5 for details. As shown in Figure 5.11 the EMI shielding behavior of all Ni@M20 samples fluctuates across the entire frequency range. This fluctuation is attributed to the porous structure of the fibrous materials, which influences mechanisms such as scattering, absorption, and reflection. Notably, with increasing nickel deposition, the electromagnetic shielding effectiveness (EM SE) at 30 MHz improves from 58.1 dB to 61.4 dB, further enhancing the shielding performance. This improvement is primarily due to nickel's high magnetic permeability, which enhances electromagnetic wave absorption, and the reduced surface porosity, which minimizes wave leakage. Additionally, the thicker nickel layer strengthens multiple reflection effects within the material, contributing to the overall increase in shielding effectiveness.

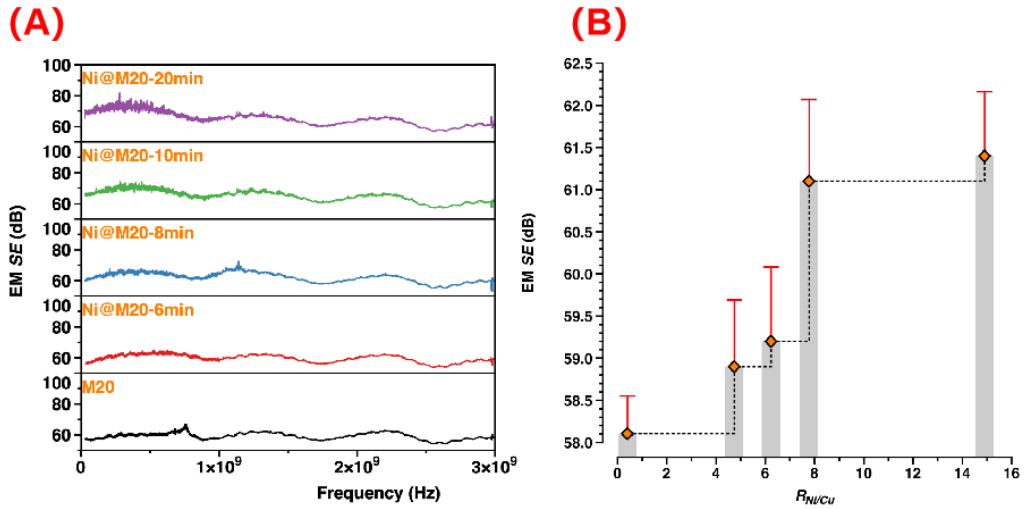

Figure 5.11 (A) EMI shielding property (B) EM *SE* at 3MHz

Table 5.5 Electrical conductivity, thermal conductivity, thermal resistance, EMI shielding property and stiffness of Ni@M20 samples (mean value±95% confidence interval)

Sample code	Volume resistivity (Ω·m)	Surface resistivity (Ω)	EM *SE* (dB)	Thermal conductivity ($W\ m^{-1}\ K^{-1}$)	Thermal resistance ($m^2 \cdot K \cdot W^{-1}$)
M20	34.28±1.29	1.37±0.02	58.10±0.45	-	-
Ni@M20-6min	19.40±0.59	1.18±0.01	58.9±0.79	0.028±0.02	3.46±0.078
Ni@M20-8min	15.62±0.37	1.17±0.01	59.2±0.88	0.0308±0.01	3.82±0.24
Ni@M20-10min	14.14±0.29	1.14±0.01	61.1±0.97	0.033±0.02	4.06±0.13
Ni@M20-20min	9.95±0.04	1.13±0.01	61.4±0.76	0.036±0.02	4.9±0.088

5.5 Effect of Ni deposition on air permeability, thermal conductivity, and thermal resistance of Ni@Cu-coated PET fabrics

Thermal comfort is a critical consideration for wearable materials, reflecting the balance between heat transfer and air permeability, which directly impacts user comfort. The deposition of nickel significantly influences the thermal properties of Ni@Cu-coated PET fabrics, including their air permeability, thermal conductivity and thermal resistance.

Figure 5.12 (A) illustrates the air permeability of Ni@M20 samples. With $R_{Ni/Cu}$ value increases from 0 to 14.5, which reflects the increasing nickel content, the air permeability of Ni@M20 samples decrease significantly from 34308 $l.m^{-2}.s^{-1}$ to 27288 $l.m^{-2}.s^{-1}$ when ΔP is at 100 Pa (for clothing applications), and decreases from 56304 $l.m^{-2}.s^{-1}$ to 43164 $l.m^{-2}.s^{-1}$ when ΔP is at 200 Pa (for industrial textile applications).

By combining it with porosity analysis in the previous sections, the reduced surface porosity of Ni@M20 samples with higher $R_{Ni/Cu}$ value results in less penetration for air flow. Besides, the exponential function can easily predict the change of air permeability of Ni@M20 samples with $R_{Ni/Cu}$ value.

Compared to our previous group study on Py15/Cu/PET (GSM 50.72 g/m²), which involved copper plating on the same substrate (MILIFE) and achieved an air permeability of 18785 $l.m^{-2}.s^{-1}$ at 200 Pa [36], the current results demonstrate significantly higher air permeability. Furthermore, when compared with other studies, such as the polyester/viscose blended needle-punched nonwoven fabric (areal density of 50.40 g/m²) with an air permeability of 42498 $l.m^{-2}.s^{-1}$, or a areal density of 99.87 g/m² fabric with an air permeability of 28 $l.m^{-2}.s^{-1}$ at 100 Pa, our samples exhibit competitive performance [37].

As shown in Figure 5.12 (B), the thermal conductivity of Ni@M20 samples increases from 0.028

$W \cdot m^{-1} \cdot K^{-1}$ (thickness 0.098 mm) to 0.036 $W \cdot m^{-1} \cdot K^{-1}$ (thickness 0.178 mm) as the $R_{Ni/Cu}$ value rises from 0 to 14.5. Correspondingly, Figure 5.12 (C) shows the thermal resistance increases from 3.50 $K \cdot m^2 \cdot W^{-1}$ to 4.94 $K \cdot m^2 \cdot W^{-1}$, indicating that while a higher nickel content enhances thermal conductivity, the increase in thickness contributes to greater overall thermal resistance. Detailed values of both thermal conductivity and thermal resistance are provided in Table 5, while thickness information is available in Table 4.2.

Given that the thermal conductivity of air is 0.025 $W \cdot m^{-1} \cdot K^{-1}$, this relatively low conductivity of Ni@M20 samples were attributed primarily to the porous structure and thin thickness of the samples. Additionally, for very thin fabrics (e.g., less than 0.5 mm), the thermal conductivity may be too low to provide stable and accurate readings due to rapid heat transfer in the ALAMBETA sensor.
Although nickel deposition enhances thermal conductivity, and its variation with coating time follows a simple exponential function, the material's inherent porosity remains the dominant factor limiting heat transfer, as indicated by the ALAMBETA measurements. In contrast, thermal resistance increases linearly with coating time, reflecting the combined effects of increasing material thickness and the reduced insulating effect of air within the porous structure.

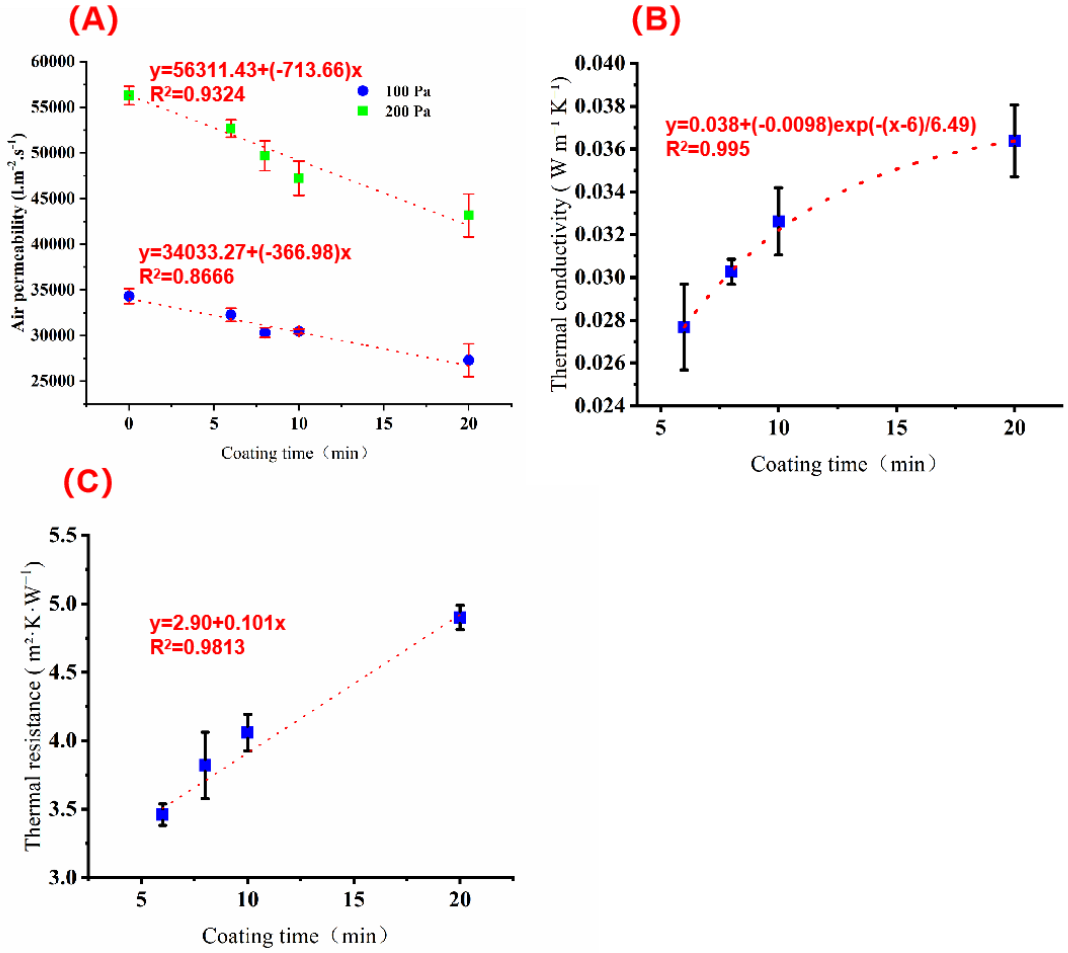

Figure 5.12 (A) air permeability and (B) thermal conductivity (C) thermal resistance of Ni@M20 samples

5.6 Thermoelectrical (TE) property of Ni@Cu-coated PET fabrics

As described in the sample preparation section, Ni@M20 samples with four different electroplating

times (*t*) were prepared. Due to their non-uniform fibrous structure (nonwoven fabric), various dimensions were considered to evaluate TE behavior. Four widths (*w*) were selected: 1 cm, 1.5 cm, 2 cm, and 5 cm, resulting in 16 samples in total. The samples are labeled as Ni@M20-t-w, where t represents the electroplating time and www the width. For example, Ni@M20-6min-1cm refers to a fiber-based Cu-coated fabric (MEFTEX20) electroplated with Ni for 6 minutes and having a width of 1 cm.

5.6.1 Comparison of continuous cooling and controlled temperature model

To evaluate the TE performance of samples, a circuit was designed. As shown in Figure 5.13 (A) and (B), the Ni@Cu-coated PET fabric samples consist of three parts: *Part 1* and Part 3 are Cu-coated PET fabric (M20), while *Part 2* is the Ni@M20 sample. Part 1 is connected to *Part 2*, and *Part 2* is connected to *Part 3*. The TE property is assessed by heating the connection between *Part 1* and *Part 2*, labeled as T_1, while the connection between *Part 2* and *Part 3* serves as the cold end with temperature T_2. The temperature difference, T_d=T_1−T_2, drives the thermoelectric effect.

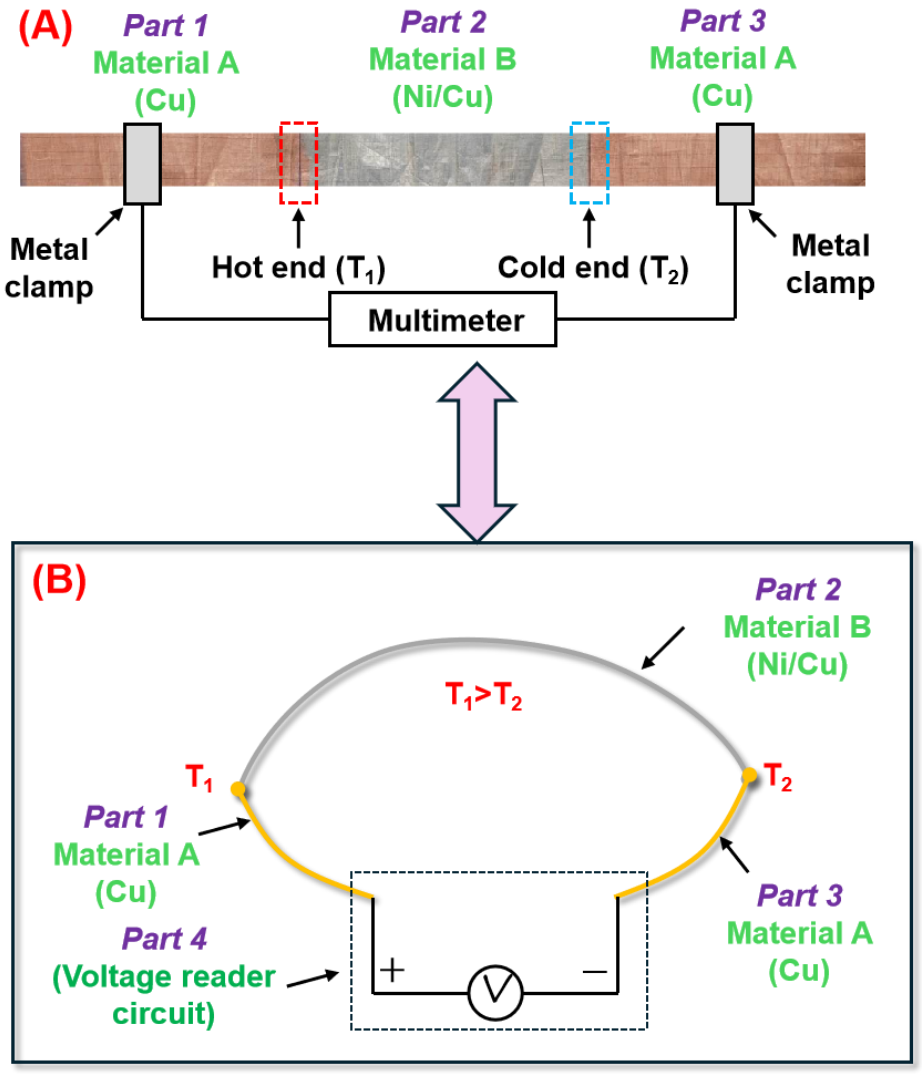

Figure 5.13 Scheme for measurement of TE property of Ni@Cu-coated PET fabrics

To achieve the experimental goals, we designed two testing setups: a continuous cooling model and a controlled temperature model. The continuous cooling model was used to observe thermoelectric

behavior across the full temperature difference T_d range, spanning 11.5 °C to 110 °C. In contrast, the controlled temperature model focused on precise regulation of the hot and cold ends, with a T_d range from 14 °C to 62 °C.

As shown in Figure 5.14 (A), (B), (C), and (D) represent the V-T_d curves for Ni@M20-6min-1cm, Ni@M20-8min-1cm, Ni@M20-10min-1cm, and Ni@M20-20min-1cm under continuous cooling and controlled temperature models, respectively. The simple linear fitting was also applied to obtain quantitative analysis of the relationship between voltage and temperature difference.

For the Ni@M20-6min-1cm sample, the *V*-T_d relationship is different under two measurement methods. This discrepancy is primarily due to the non-uniformity of the sample. In the controlled temperature model, the uniform temperature distribution at the hot and cold ends compensates for these inconsistencies, resulting in higher voltage output. In contrast, the continuous cooling model, with its transient temperature gradients, is more affected by sample non-uniformity, leading to a lower observed voltage. For the Ni@M20-8min-1cm sample, the discrepancy between the controlled temperature model and continuous cooling models is reduced. For the 10min-1cm and 20min-1cm samples, the discrepancies between the controlled temperature model and continuous cooling models were minimal. By combining structural analysis, the increased electroplating time results in a more uniform Ni deposition layer, which provides precise control of TE behavior.

The comparison revealed that for most samples, the controlled temperature model data from the controlled temperature model aligned closely with the data obtained from the continuous cooling model, with only minor deviations. This consistency demonstrates that the continuous cooling model accurately captures thermoelectric behavior under controlled temperature model conditions, providing a reliable and practical approach for characterizing thermoelectric materials, especially across a broader T_d range.

Overall, the strong agreement between the two models supports the use of the continuous cooling model for thermoelectric analysis, except for specific conditions where sample structure or temperature distribution might influence the results.

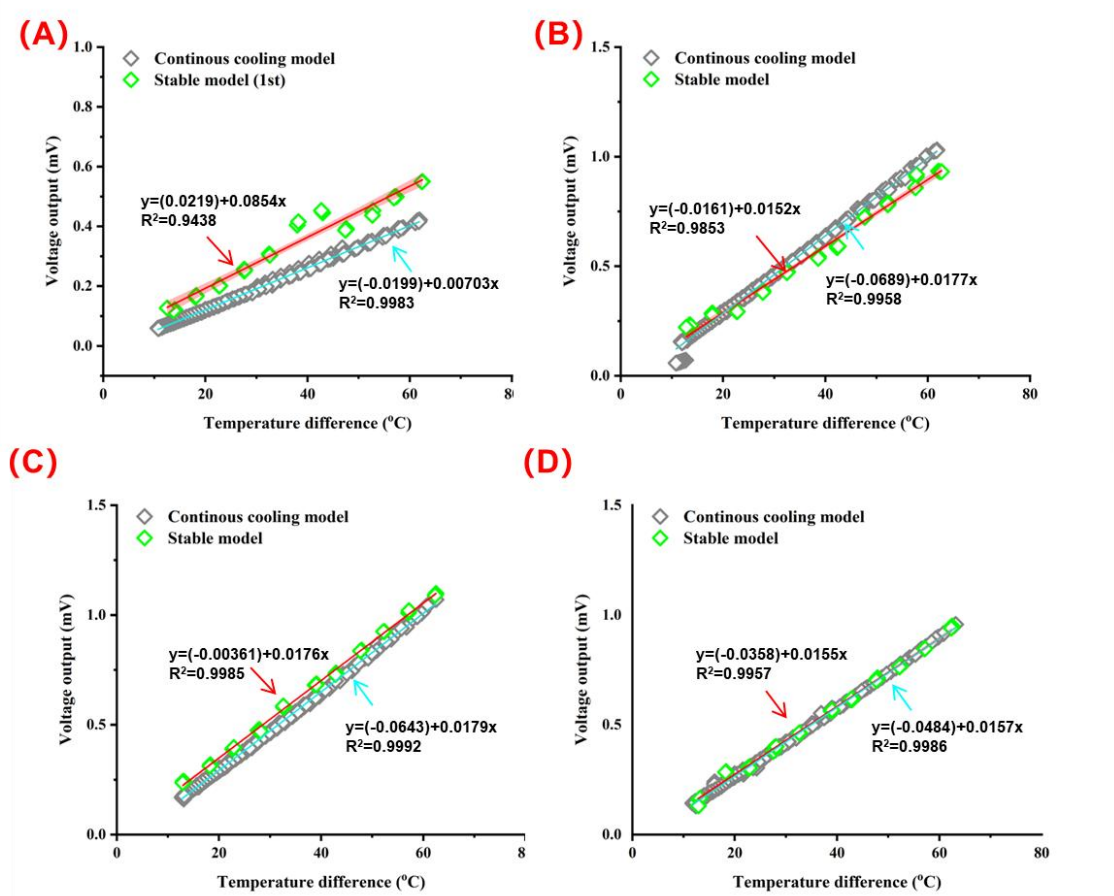

Figure 5.14 Comparison of V-T_d curves for Ni@Cu-coated PET samples under continuous cooling and controlled temperature model models (A: Ni@M20-6min-1cm BCD correspond to, Ni@M20-8min-1cm, Ni@M20-10min-1cm, and Ni@M20-20min-1cm samples, respectively.)

Building on the comparison of the two testing models, the continuous cooling data is now exclusively used to perform mathematical modeling and analyze the thermoelectric behavior of the Ni@Cu-coated PET fabric. The V-T_d curves over the range from 11.5 °C to 110 °C for the Ni@Cu-coated PET fabric with a width of 1 cm is presented in Figure 5.15. The value of V was found to increase steadily with rising V-T_d across the range of 11.5 °C to 110 °C. For the Ni@Cu-coated PET fabric samples, the maximum thermoelectric voltage ranged between 1.3 mV and 2 mV. To demonstrate the unique advantages of our samples, a Ni@Cu foil sample was also prepared using the same electroplating process. However, as shown in the V-T_d curve in Figure 5.15, the Ni@Cu foil displayed almost no thermoelectric properties. The thermoelectric (TE) performance of both foil-based and fiber-based samples is influenced by their structural characteristics and the resulting electron transport pathways:

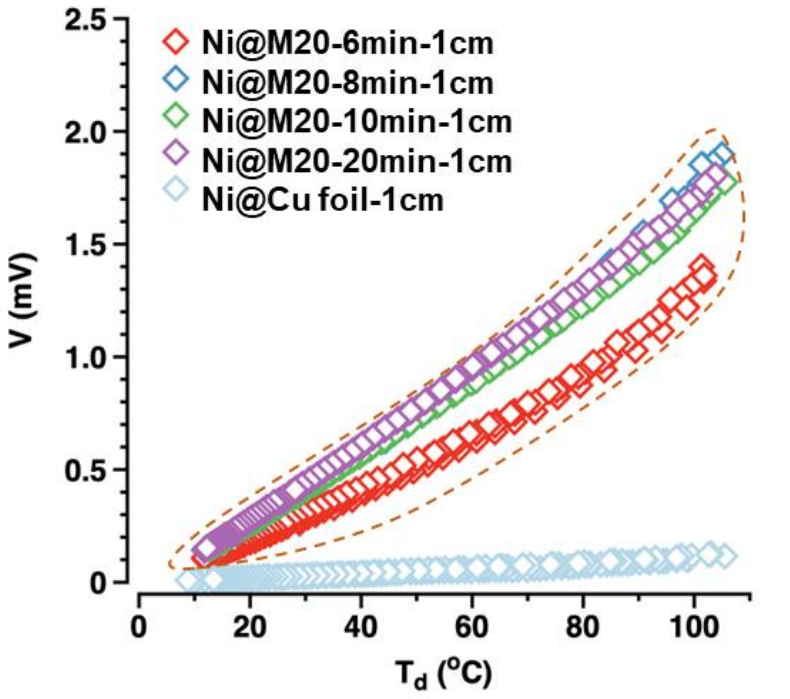

Figure 5.15 Measured V-T_d curves

- TE Behavior of Ni@Cu Foil

The poor thermoelectric (TE) performance of Ni@Cu Foil is mainly caused by an electronic carrier "shortcut." While Ni and Cu exhibit differences in Fermi energy levels and Seebeck coefficients (e.g., -20 μV/K for Ni and 2.5 μV/K for Cu), the high thermal and electrical conductivity of Cu enables the electronic carriers generated by thermoelectric electromotive force (*emf*) to move freely. This leads to the formation of an electronic carrier "shortcut," as depicted in Figure 5.16.

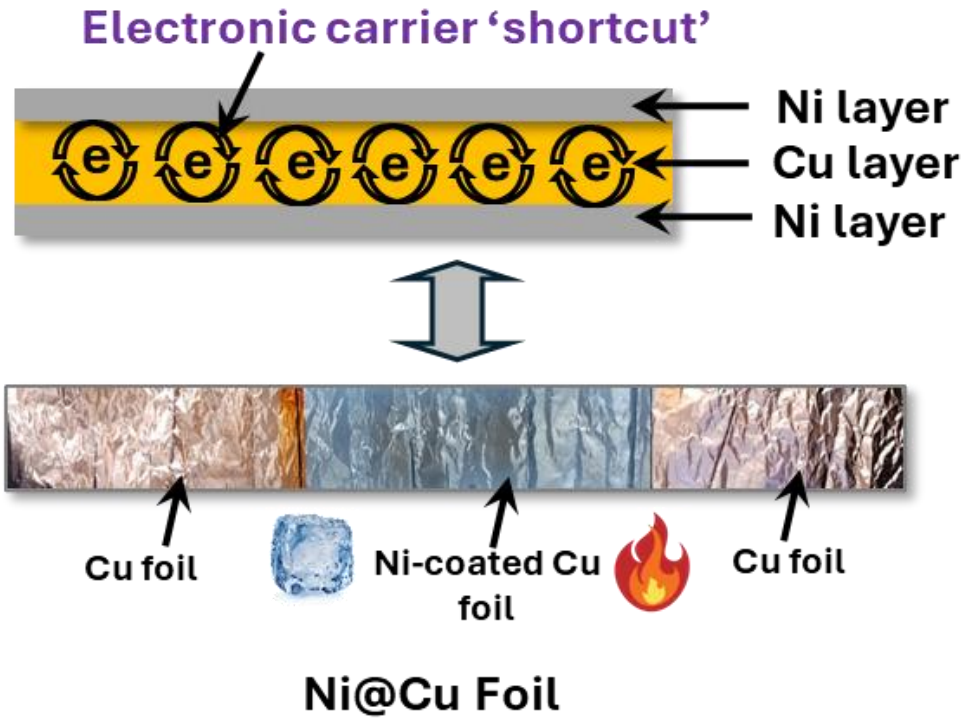

Figure 5.16 Mechanism for TE phenomena of Ni@Cu Foil

- TE behavior of Ni@Cu-coated PET fabric samples

In contrast, Ni@Cu-coated PET fabric samples demonstrate a significant reduction in electron carrier shortcuts, as depicted in Figure 5.17. This improvement can be attributed to two main factors:

1) Higher resistance from Cu oxides: The Cu oxides within the Cu chemical deposition layer introduce higher internal resistance, effectively limiting the movement of electron carriers. As a result, the electron carriers generated by the electromotive force (*emf*) are more likely to follow the temperature distribution.

2) Nanoscale effect coupled with porous fiber structure: The presence of Cu and Ni nanoparticles, deposited on the porous structure of the PET fibers, enhances phonon scattering. The interconnected porous structure not only supports the dispersion of nanoparticles but also aids in reducing lattice thermal conductivity by amplifying heat-carrying phonon scattering. This synergy between the nanoscale effects and the porous architecture effectively minimizes electron carrier shortcuts and significantly boosts thermoelectric performance.

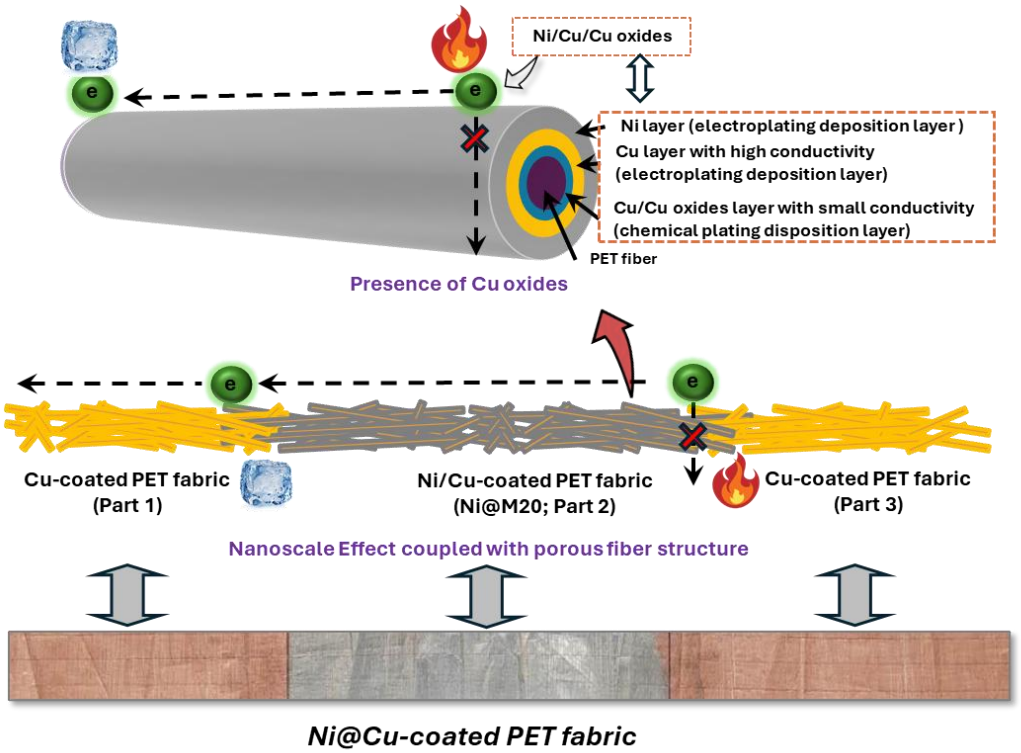

Figure 5.17 Mechanism for TE phenomena of Ni@Cu-coated PET fabric

5.6.2 Adjusting TE property of Ni@Cu-coated PET fabric

The thermoelectric (TE) properties of Ni@Cu coated PET fabrics are shown above Figure 5.18 (A). However, the voltage (V) does not increase linearly with the temperature difference T_d across the entire T_d range [30]. To evaluate the TE performance, the Seebeck coefficient (S) is typically used, calculated as dV/dT. This value is derived from the linear portion of the V-T_d curve when T_d falls

within a specific limited range, see Figure 5.18 (B).

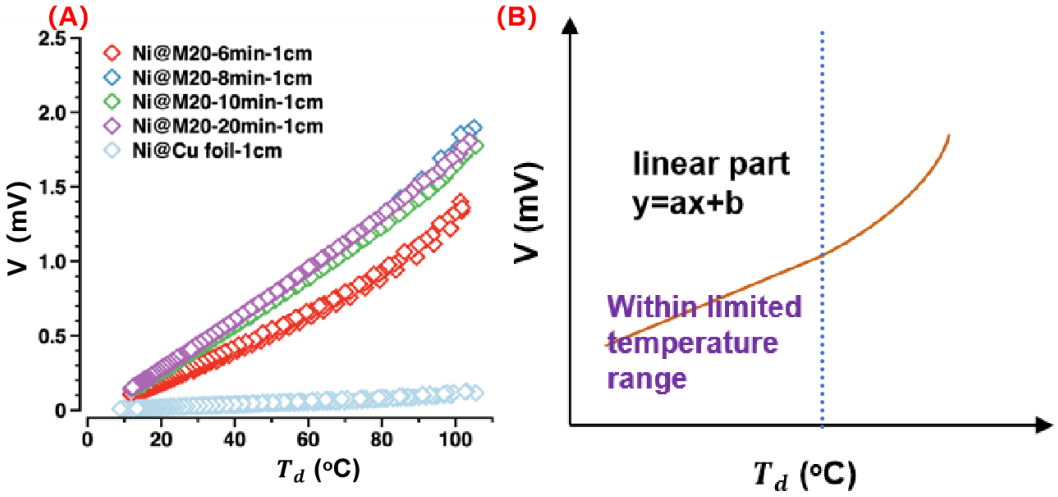

Figure 5.18 (A) *V*-T_d curves (B) of fiber-based Ni@Cu-coated PET fabric, linear part of *V*-T_d curves when temperature range is limited

After observing *V*-T_d curves of Ni@Cu-coated PET fabric and considering practical usage for human (e.g., thermal protection or thermal management), the T_d of 58 °C is selected as critical point, and a simple linear relationship y=ax+b is applied for Ni@Cu-coated PET fabric by fitting T_d range [11.58,58],which is shown in the Figure 5.19. By taking sample Ni@M20-8min-1cm, good fitting of y=ax+b is found by having R^2 value reaches 0.9996 and random residual distribution. As a result, y=ax+b can be applied, pre-factor 'a' is the *S* value, and the *S* value of sample Ni@M20-8min-1cm is 0.017 mV/K (17μV/K).

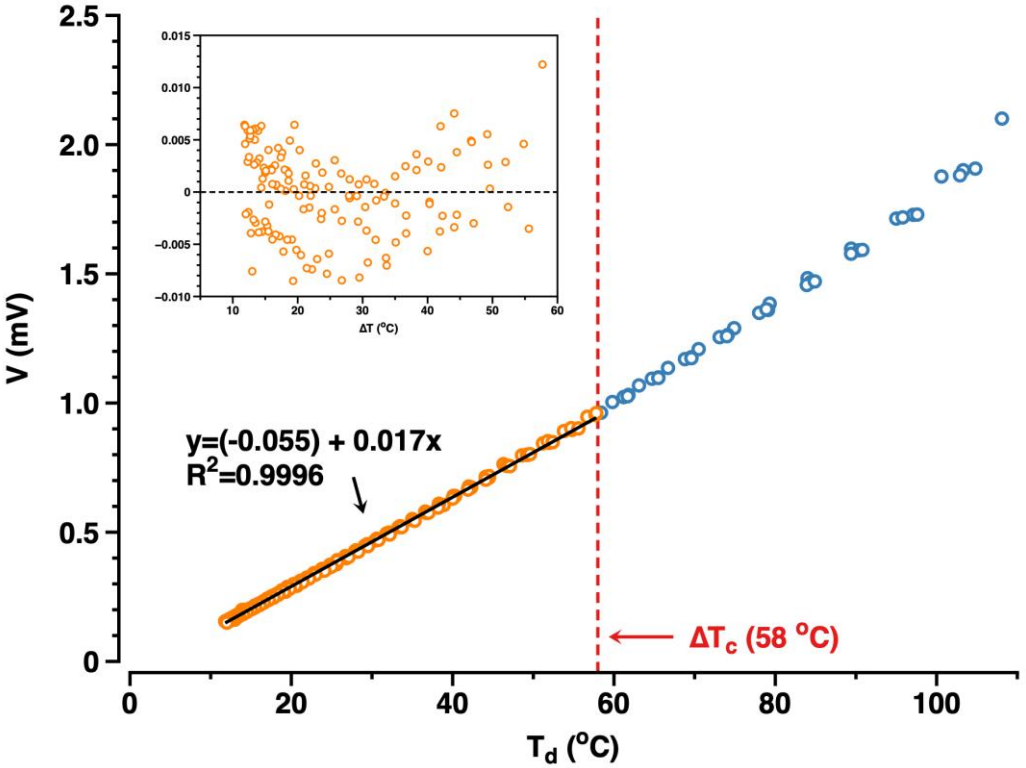

Figure 5.19 Linear fitting in limited ΔT range for sample Ni@M20-8min-1cm

Based on the analytical techniques, the thermoelectric properties of all Ni@Cu-coated PET fabrics were analyzed consistently. Figure 5.20 shows the V-T_d curves of Ni@M20-6min, Ni@M20-8min, Ni@M20-10min and Ni@M20-20min with different widths (w). The Seebeck coefficients of the samples were determined by linearly fitting the slopes obtained within the temperature difference range $T_d \in [11.5, 58]$.

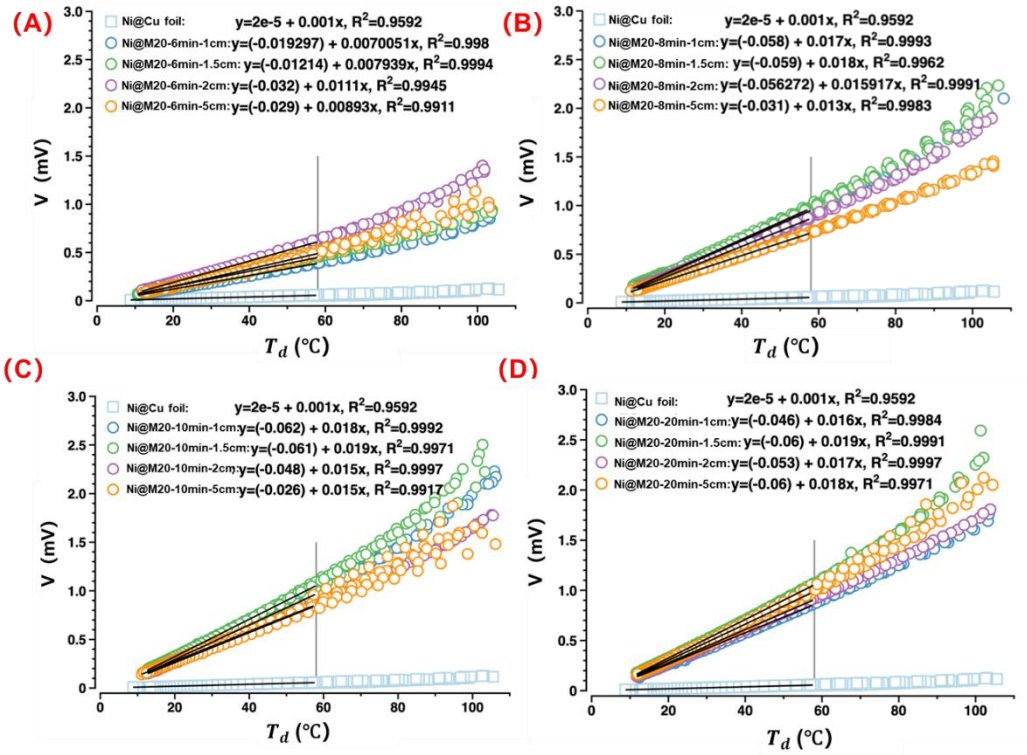

Figure 5.20 Thermoelectrical property of Ni@Cu-coated PET fabric and Ni-coated Cu film according to continuous cooling model measurement (A, B, C and D: Ni@M20-6min, Ni@M20-8min, Ni@M20-10min and Ni@M20-20min)

Figure 5.21 shows the relationship between the estimated Seebeck coefficient (S) and the mass ratio $R_{Ni/Cu}$ across all samples with varying widths (w). Subplots display S values as functions of $R_{Ni/Cu}$ for different Ni plating times (t) and widths. Since S is an intrinsic material property, it should theoretically depend only on the material composition and temperature difference, not on width. However, the observed impact of w on S is mainly due to the randomness of the nonwoven substrate and inconsistencies in deposition during preparation.

Compared to w value, $R_{Ni/Cu}$ plays a more significant role in determining S. To address variations caused by w value, statistical processing was applied to the S values. For samples Ni@M20-6min-1cm, Ni@M20-8min-1cm, Ni@M20-10min-1cm, and Ni@M20-20min-1cm, the S values are is 8.75 ± 1.48 μV/K, 16 ± 2.12 μV/K, 16.75 ± 2.20 μV/K, 17.5 ± 1.29 μV/K, respectively. This demonstrates that S improves with an increase in $R_{Ni/Cu}$, emphasizing the role of composition in enhancing thermoelectric performance.

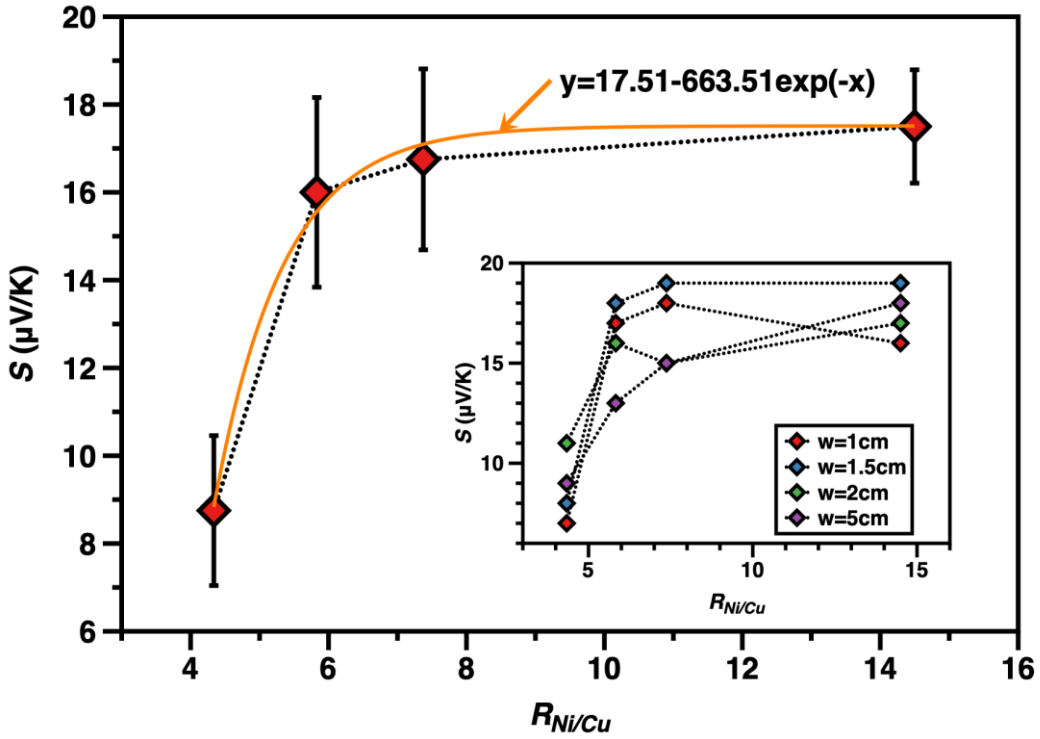

Figure 5.21 Change of Seebeck coefficient with $R_{Ni/Cu}$ and width

5.6.3 TE stability of Ni@Cu-coated PET fabrics under different conditions

The long-term reliability and durability of thermoelectric (TE) materials are critical for their practical application, particularly in scenarios involving dynamic or harsh environments. For Ni@Cu-coated PET fabrics, understanding how their TE properties respond to various conditions, such as mechanical deformation, environmental exposure, and repeated usage, is essential for assessing their feasibility in real-world applications. This section evaluates the TE stability of these materials under bending and twisting states, exposure to wind and after washing providing a comprehensive understanding of their performance in practical scenarios.

The original thermoelectric performance of the sample M20-8min-1cm was measured in its straight, undeformed state, resulting a Seebeck coefficient (*S*) of 17 μV/K (Figure 5.22(A)). This serves as the reference point for comparing the effects of different conditions.

5.6.3.1 TE stability of sample with bending

When the sample was bent into a 'Λ' shape, forming a 90° angle, the *S* value slightly decreased to 16 μV/K (Figure 5.22 (B)). This minor change indicates that bending has little impact on the thermoelectric properties, consistent with the principle that thermoelectric performance is not affected by shape deformation.

5.6.3.2 TE stability of sample with twisting

When the sample was twisted at 2 turns per 20 cm (2T/20cm), the *S* value remained at 16 μV/K (Figure 5.22 (C)). This shows that twisting also has a minimal influence on the thermoelectric behavior, demonstrating the fabric's stability in maintaining TE performance under various

configurations.

5.6.3.3 TE stability of sample under heat convection

The heat convection is adjusted by controlling wind speed. Under a wind speed of 2 m/s, the *S* value increased slightly to 18 μV/K (Figure 5.22 (D)). This slight increase can be attributed to enhanced heat convection, which reduces heat transfer from the hot end to the cold end. Despite this variation, the *S* value remains close to the baseline, confirming the fabric's stability under airflow conditions.

These results confirm that the Ni@Cu-coated PET fabric exhibits high TE stability under various situations, making it a reliable material for practical applications.

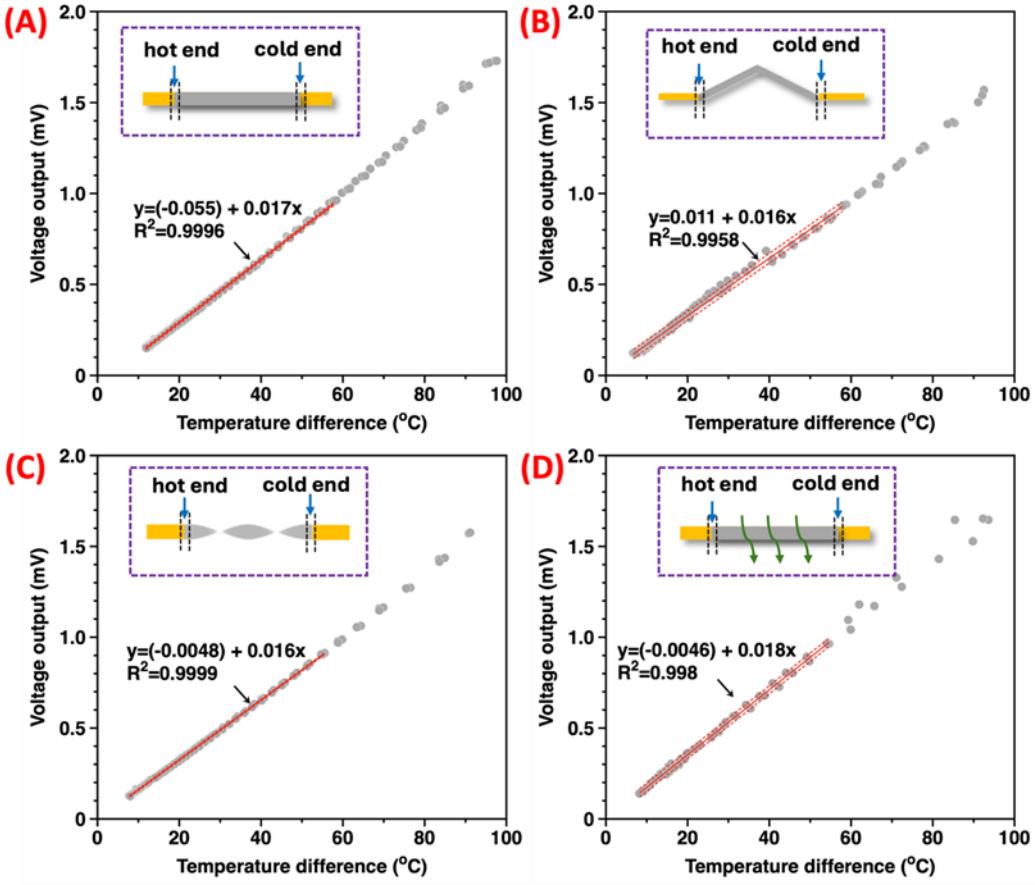

Figure 5.22 (A) Thermoelectrical property with linear fit of sample Ni@M20-8min-1cm (A), (B) sample Ni@ M20-8min-1cm with 'Λ' shape, (C) twisted sample Ni@M20-8min-1cm according to common continuous cooling method, (D)sample Ni@M20-8min-1cm according to continuous cooling method with wind speed of 2 m/s (fitting range: x∈(0,58), and red dash: 95 % confidence interval)

5.6.3.4 TE behavior after washing

In earlier chapters, the Seebeck coefficient of the Ni@M20-20min sample was identified as the most uniform and optimal, with an average value of 17.5±1.29 μV/K across its width. Ni@M20-20min-1cm was selected to evaluate performance before and after washing. The weight loss percentage of the sample during the washing process was approximately 0.14%, confirming that material loss was minimal. Figure 5.23 shows the comparison of thermoelectric performance before and after washing

for Ni@M20-20min-1cm.

Following 30 minutes of washing, the slope (estimated Seebeck coefficient) of the Ni@M20-20min-1cm sample increased slightly, from 15.7±0.06 μV/K (pre-washing), to 16.9±0.05 μV/K (after-washing). This indicates an improvement in thermoelectric performance. The observed increase in the Seebeck coefficient is likely attributed to surface cleaning, oxide layer formation, or improved interfacial properties, which collectively enhance the material's thermoelectric response. However, the change in Seebeck coefficient, while measurable, may not be statistically significant given the narrow error margins and small variation.

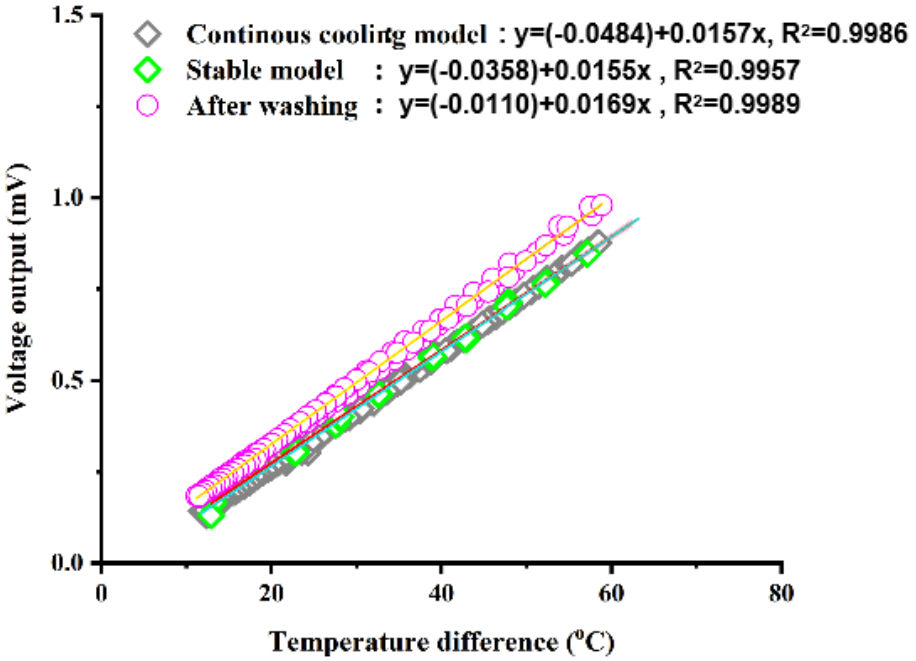

Figure 5.23 Comparison of thermoelectric performance before and after washing for Ni@M20-20min-1cm

5.6.3.5 Fast thermoelectric response of Ni@Cu-coated PET fabric

While the thermoelectric (TE) properties of the Ni@Cu-coated PET fabric have been the primary focus, including its enhanced Seebeck coefficient and improved TE performance, these properties alone do not fully determine its applicability in thermocouple (TC) applications. A key performance metric for TCs is their response time, which reflects how efficiently the material converts temperature changes into electrical signals in practical scenarios [38–41]. Understanding the response time not only complements the analysis of TE properties but also provides a crucial link to real-world usability, making it essential to investigate both aspects comprehensively.

The response of Ni@Cu-coated PET fabric is characterized by time constant ($t_{0.63}$) and response time ($t_{0.93}$). The $t_{0.63}$ (s) is defined as the time required for thermocouple (TC) to respond to 63.2% of its total output signal ($V_{0.63}$) when there is a temperature change of hot end [42–44]. The $t_{0.93}$ is the whole time required for TC to respond to 93% of its total output signal ($V_{0.93}$) when there a temperature change of hot end. To determine $t_{0.63}$ and $t_{0.93}$, the 1% maximum voltage output ($V_{0.01}$) with time $t_{0.01}$ is selected as beginning point by considering errors. Although higher Ni deposition

on the Ni@Cu-coated PET fabric samples results in better thermal conductivity and electrical conductivity, it could cause a small influence on response.

As shown in Figure 5.24, the sample Ni@M20-8min-1cm is measured 3 times. the average $t_{0.63}$ value of sample Ni@M20-8min-1cm with T_d of 5 ºC is about 2.5 s, and the average $t_{0.93}$ value of sample Ni@M20-8min-1cm with T_d of 5 ºC is about 4.2 s. By referring to the response behavior of common thermocouple with or without insulated material, the Ni@Cu-coated PET fabric could have a faster response.

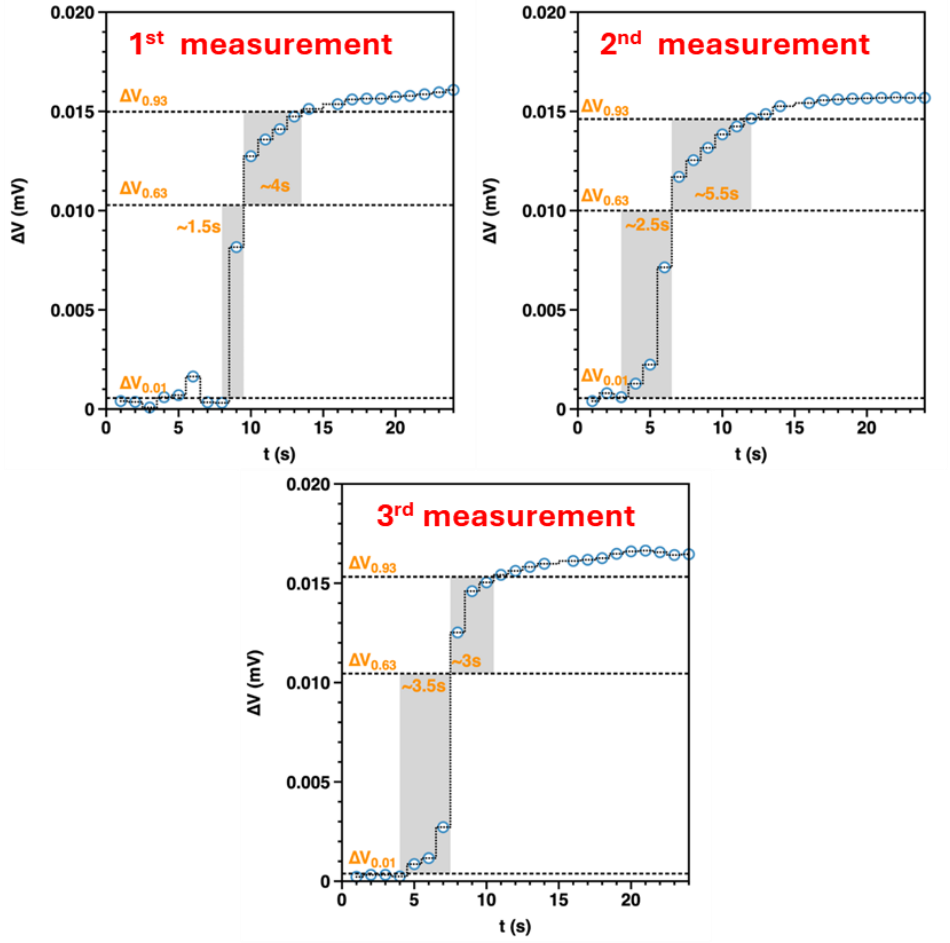

Figure 5.24 Voltage output (V) response behavior of sample Ni@M20-8min-1cm with temperature difference (T_d) of 5 ºC

5.6.4 Comparison with current work

Film-based thermoelectric materials have long been regarded as foundational platforms due to their high performance, uniformity, and stability, making them ideal for rigid systems and well-established applications [39,40]. In contrast, fiber-based thermoelectric materials represent a novel class, offering significant advantages such as lightweight, flexibility, and adaptability to irregular surfaces. These properties make fiber-based materials particularly suitable for wearable electronics and other portable applications.

To better illustrate the advantages of our Ni@Cu-coated PET fabric, we compare its S value with those of current metal-incorporated flexible thermoelectric materials, including both fiber-based TE materials (Cu/Ni-FiBTEM) and film-based TE materials (Cu/Ni-FBTEM). It is important to note

that the overall S value in some studies is achieved using multiple TE pairs. Since our research focuses on a metal-based material with only one TE pair, we have limited our comparison to studies reporting metal-based thermoelectric materials with a single TE pair. The highest S values from these works are summarized in Table 5.6.

As a result, the S value of the Ni@Cu-coated PET fabric(this work) is lower than that of most metal-incorporated flexible TE materials, primarily due to material selection. However, the S value achieved in this work is comparable to that of Cu/Ni-FBTEM and higher than other Cu/Ni-FiBTEM. By considering the advantages and limitations of current technologies and flexible TE materials, the following key points outline the potential for industrial production of the Ni@Cu-coated PET fabric.

- Comparison with current Cu/Ni-film based flexible TE materials (Cu/Ni-FBTEM)

The current Cu/Ni-FBTEMs offer some flexibility; however, their application is limited by the thickness of the TE legs or the substrate [31]. In comparison, the Cu/Ni-coated PET fabric developed in this work eliminates the issue of a limited bending radius, thanks to its fibrous structure. Additionally, the porous nature of this material provides enhanced thermal comfort, making it more suitable for wearable applications.

- Comparison with current Cu/Ni fiber-based TE materials (Cu/Ni-FiBTEM)

Compared to current Cu/Ni-FiBTEM, the fabrication of Ni@Cu-coated PET fabric is more straightforward and easier to realize. This is due to its simple structure, which is developed using an electroplating method on commercially available Cu-coated PET fabric. The electroplating process offers a highly efficient and scalable production approach, making it more practical and cost-effective compared to other fabrication methods.

Table 5.6 Comparison in Seebeck coefficient (*S*) of this work with other metal-based flexible TE materials

Type	Substrate	TE materials	*S* value	Method	Reference
Film-based TE materials	PI	Pt/In_2O_3	204.4	Magnetron sputtering	[45]
	PI	Cu/Ni	8.9	Magnetron sputtering	[46]
	PI	Cu/CuNi	42	Magnetron sputtering	[27]
	PI	Cu/CuNi	30.6	Aerosol jet printing	[24]
	PI film	Cu/CuNi	20.6	Aerosol jet printing	[47]
	Kapton substrates	Cu/CuNi	43.7	Aerosol jet printing	[25]
	PI	Cu/CuNi	40	Aerosol jet	[25]

				printing	
	PI	Cu/CuNi	22.3	Evaporation	[48]
	PEN and Kapton	BST/Cu	124	Printing	[49]
	PEN and Kapton	BST/BT	319	Printing	[49]
	PET	C/Ag	9	Printing	[50]
	PET	Ag/Ni	16	Printing	[50]
	PET	C/Ni	27	Printing	[50]
Fiber-based TE materials	Cotton fabric	Cu-Ni/Ag-F	45.3	Weaving	[51]
	Carbon fabric	Bi_2Te_3 coated Ni-Cu	4.7	Drop-casting	[52]
	PET fabric	Alumel/CuI	220	SILAR	[53]
	Carbon fiber	C-Ni	12.6	Electroplating	[51]
	PEG fabric	Ni/Cu	17.5	Electroplating	This work

C: carbon fiber; PI: polyimide; PEN: polyethylene naphthalate two formic acid glycol esters; PET: polyester; SILAR: successive ionic layer adsorption and reaction

6 Conclusion

In this work, nickel (Ni)-coated copper (Cu)-coated polyester nonwoven fabrics (Ni@Cu-coated fabrics) were successfully fabricated using electroplating technology, with the copper layer formed through a combination of chemical plating and electroplating. The amount of nickel deposition was precisely controlled by adjusting the electroplating time. Comprehensive characterization, including morphological, compositional, and structural analyses, was conducted to evaluate the samples.

Morphological characterization revealed that the nickel coating gradually covered the copper layer and filled the fabric pores with increasing electroplating time. The thickness of both nickel and copper layers was confirmed to be nanoscale, exhibiting a uniform and compact structure. Crystal structure and valence state analysis results indicated the presence of copper oxides in the copper layer, particularly in the chemical plating region, and nickel oxides in the nickel coating. These oxides contribute positively to the material's thermoelectric performance.

Compared to conventional nickel electroplating on copper foils, which often leads to short-circuiting, the Ni@Cu-coated fabrics fabricated in this study significantly reduced short-circuit risks. This improvement was attributed to the nanoscale distribution of nickel and copper particles, as well as the presence of copper oxides, which enhanced the material’s electrical conductivity and stability.

To characterize thermoelectric materials, two testing setups were developed: a continuous cooling model for wide temperature ranges (11.5 °C to 110 °C) and a controlled temperature model for precise regulation (14 °C to 62 °C). Results showed strong consistency between the two methods, validating the continuous cooling model as a reliable approach for controlled temperature model thermoelectric characterization across broad temperature differences. Thermoelectric performance evaluation demonstrated that the Seebeck coefficient remained stable within the range of 8.75 to 17.50 μV/K across a wide temperature difference (T_d) range of 11.5 °C to 110 °C. The performance remained consistent under various conditions, including indoor continuous cooling, twisting, wind exposure, and after washing. The rapid thermoelectric response of the material was evidenced by a time constant ($t_{0.63}$) and response time ($t_{0.93}$) of 2.5 seconds and 4 seconds, respectively, under a temperature difference of 5 °C.

In addition to its excellent thermoelectric performance, the Ni@Cu-coated fabrics demonstrated superior flexibility, electromagnetic shielding, and thermal comfort properties. The material’s breathability, softness, and comfort make it a promising candidate for smart wearable thermocouple applications.

7 References

[1] C. Goupil, H. Ouerdane, K. Zabrocki, W. Seifert, N.F. Hinsche, E. Müller, Thermodynamics and Thermoelectricity, Contin. Theory Model. Thermoelectr. Elem. (2016) 1–74. https://doi.org/10.1002/9783527338405.CH1.

[2] H. Hardianto, G. De Mey, B. Malengier, L. Van Langenhove, Textile-based thermoelectric generator fabricated from carbon fibers, J. Ind. Text. 51 (2022) 8411S-8427S. https://doi.org/10.1177/1528083720910686.

[3] S. Kim, S. Lim, M.H. Jeong, W. Kim, S. Baik, J.W. Suk, Flexible thermocouple using a thermoelectric graphene fiber with a seamless junction, J. Mater. Sci. Technol. 172 (2024) 15–22. https://doi.org/10.1016/J.JMST.2023.05.078.

[4] C. Anderson, Z.H. Fan, J. Richstein, M. Sussman, T. Nishida, A Comparison of Relative Seebeck Coefficients for Screen Printed Flexible Thermocouples Using Commercially Available Conductive Inks, FLEPS 2023 - IEEE Int. Conf. Flex. Printable Sensors Syst. Proc. (2023) 1–4. https://doi.org/10.1109/FLEPS57599.2023.10220389.

[5] Y. Cui, X. He, W. Liu, S. Zhu, M. Zhou, Q. Wang, Highly Stretchable, Sensitive, and Multifunctional Thermoelectric Fabric for Synergistic-Sensing Systems of Human Signal Monitoring, Adv. Fiber Mater. 6 (2024) 170–180. https://doi.org/10.1007/S42765-023-00339-8/FIGURES/5.

[6] Y. Song, H. Yu, Y. Ran, H. Zeng, W. Li, J. He, K. Tai, Z. Yu, High-performance flexible wavy-structure thermoelectric generator based on (Bi, Sb)2Te3 films for energy harvesting, J. Power Sources. 600 (2024) 234260. https://doi.org/10.1016/j.jpowsour.2024.234260.

[7] X. Zhu, Y. Yu, F. Li, A review on thermoelectric energy harvesting from asphalt pavement: Configuration, performance and future, Constr. Build. Mater. 228 (2019) 116818. https://doi.org/10.1016/J.CONBUILDMAT.2019.116818.

[8] D. Shiojiri, T. Iida, H. Kakio, M. Yamaguchi, N. Hirayama, Y. Imai, Enhancement of thermoelectric performance of Mg2Si via co-doping Sb and C by simultaneous tuning of electronic and thermal transport properties, J. Alloys Compd. 891 (2022) 161968. https://doi.org/10.1016/J.JALLCOM.2021.161968.

[9] G.K. Goyal, T. Dasgupta, Fabrication and testing of Mg2Si1-xSnx based thermoelectric generator module, Mater. Sci. Eng. B. 272 (2021) 115338. https://doi.org/10.1016/J.MSEB.2021.115338.

[10] T. Dias, A. Ratnayake, Integration of micro-electronics with yarns for smart textiles, Elsevier Ltd., 2015. https://doi.org/10.1016/B978-0-08-100201-8.00006-0.

[11] Z. Lu, H. Zhang, C. Mao, C.M. Li, Silk fabric-based wearable thermoelectric generator for energy harvesting from the human body, Appl. Energy. 164 (2016) 57–63. https://doi.org/10.1016/j.apenergy.2015.11.038.

[12] M.K. Kim, M.S. Kim, S.E. Jo, H.L. Kim, S.M. Lee, Y.J. Kim, Wearable thermoelectric generator for human clothing applications, 2013 Transducers Eurosensors XXVII 17th Int. Conf. Solid-State Sensors, Actuators Microsystems, TRANSDUCERS EUROSENSORS 2013. (2013) 1376–1379. https://doi.org/10.1109/TRANSDUCERS.2013.6627034.

[13] W. Root, T. Bechtold, T. Pham, Textile-Integrated thermocouples for temperature measurement, Materials (Basel). 13 (2020). https://doi.org/10.3390/ma13030626.

[14] D. Dupont, P. Godts, D. Leclercq, Design of Textile Heat Flowmeter Combining Evaporation Phenomena, Text. Res. J. 76 (2006) 772–776. https://doi.org/10.1177/0040517507068288.

[15] X. Chen, X. Yang, X. Han, Z. Ruan, J. Xu, F. Huang, K. Zhang, Advanced Thermoelectric Textiles for Power Generation: Principles, Design, and Manufacturing, Glob. Challenges. 8 (2024) 1–32. https://doi.org/10.1002/gch2.202300023.

[16] V. Jangra, S. Maity, P. Vishnoi, A review on the development of conjugated polymer-based textile thermoelectric generator, J. Ind. Text. 51 (2022) 181S-214S. https://doi.org/10.1177/1528083721996732.

[17] S. Shin, R. Kumar, J.W. Roh, D.S. Ko, H.S. Kim, S. Il Kim, L. Yin, S.M. Schlossberg, S. Cui, J.M. You, S. Kwon, J. Zheng, J. Wang, R. Chen, High-Performance Screen-Printed Thermoelectric Films on Fabrics, Sci. Reports 2017 71. 7 (2017) 1–9. https://doi.org/10.1038/s41598-017-07654-2.

[18] Z. Lu, M. Zhou, H. Zhang, Screen-printing Bi2S3 nanowires on silk fabrics for a flexible optical switch, Flex. Print. Electron. 2 (2017). https://doi.org/10.1088/2058-8585/aa63cc.

[19] S.J. Kim, J.H. We, B.J. Cho, A wearable thermoelectric generator fabricated on a glass fabric, Energy Environ. Sci. 7 (2014) 1959–1965. https://doi.org/10.1039/c4ee00242c.

[20] X. Liao, W. Song, X. Zhang, H. Huang, Y. Wang, Y. Zheng, Directly printed wearable electronic sensing textiles towards human-machine interfaces, J. Mater. Chem. C. 6 (2018) 12841–12848. https://doi.org/10.1039/c8tc02655f.

[21] K. Yusupov, A. Vomiero, Polymer-Based Low-Temperature Thermoelectric Composites, Adv. Funct. Mater. 30 (2020). https://doi.org/10.1002/adfm.202002015.

[22] B. Hu, X.-L. Shi, T. Cao, M. Li, W. Chen, W.-D. Liu, W. Lyu, T. Tesfamichael, Z.-G. Chen, Advances in Flexible Thermoelectric Materials and Devices Fabricated by Magnetron Sputtering, Small Sci. (2023). https://doi.org/10.1002/smsc.202300061.

[23] T. Kim, S. An, C. Park, J. Choi, A.L. Yarin, S.S. Yoon, Flexible heat-spreading and air-cooling films using nickel-electroplated nanotextured fibers, Chem. Eng. Sci. 227 (2020) 115951. https://doi.org/10.1016/J.CES.2020.115951.

[24] M.J. Renn, M. Schrandt, J. Renn, J.Q. Feng, Localized Laser Sintering of Metal Nanoparticle Inks Printed with Aerosol Jet® Technology for Flexible Electronics, J. Microelectron. Electron. Packag. 14 (2017) 132–139. https://doi.org/10.4071/IMAPS.521797.

[25] M.T. Rahman, C.Y. Cheng, B. Karagoz, M. Renn, M. Schrandt, A. Gellman, R. Panat, High Performance Flexible Temperature Sensors via Nanoparticle Printing, ACS Appl. Nano Mater. 2 (2019) 3280–3291. https://doi.org/10.1021/acsanm.9b00628.

[26] A. Leal-Junior, L. Avellar, A. Frizera, C. Marques, Smart textiles for multimodal wearable sensing using highly stretchable multiplexed optical fiber system, Sci. Rep. 10 (2020). https://doi.org/10.1038/s41598-020-70880-8.

[27] X.; Miao, X.; Gao, K.; Su, Y.; Li, Z.A. Yang, T. Flexible, A. Liu, X. Miao, X. Gao, K. Su, Y. Li, Z. Yang, A Flexible Thermocouple Film Sensor for Respiratory Monitoring, Micromachines 2022, Vol. 13, Page 1873. 13 (2022) 1873. https://doi.org/10.3390/MI13111873.

[28] Z. Zhang, Z. Liu, J. Lei, L. Chen, L. Li, N. Zhao, X. Fang, Y. Ruan, B. Tian, L. Zhao, Flexible thin film thermocouples: From structure, material, fabrication to application, iScience. 26 (2023). https://doi.org/10.1016/j.isci.2023.107303.

[29] F. Sun, H. Jiang, H. Wang, Y. Zhong, Y. Xu, Y. Xing, M. Yu, L.W. Feng, Z. Tang, J. Liu, H. Sun, H. Wang, G. Wang, M. Zhu, Soft Fiber Electronics Based on Semiconducting Polymer, Chem. Rev. 123 (2023) 4693–4763. https://doi.org/10.1021/ACS.CHEMREV.2C00720/ASSET/IMAGES/MEDIUM/CR2C00720_0036.GIF.

[30] H. Li, Y. Liu, S. Liu, P. Li, C. Zhang, C. He, Wet-spun flexible carbon nanotubes/polyaniline fibers for wearable thermoelectric energy harvesting, Compos. Part A Appl. Sci. Manuf. 166 (2023) 107386. https://doi.org/10.1016/J.COMPOSITESA.2022.107386.

[31] E. Jin Bae, Y. Hun Kang, K.S. Jang, S. Yun Cho, Enhancement of Thermoelectric Properties of PEDOT:PSS and Tellurium-PEDOT:PSS Hybrid Composites by Simple Chemical Treatment, Sci. Rep. 6 (2016) 1–10. https://doi.org/10.1038/srep18805.

[32] V. Jangra, P. Vishnoi, S. Maity, Development of polypyrrole-coated cotton thermoelectric fabrics, J. Text. Inst. 0 (2023) 1–12. https://doi.org/10.1080/00405000.2023.2223358.

[33] A. Ali, V. Baheti, J. Militky, Z. Khan, G. Zhu, Metal Coating on Ultrafine Polyester Non-woven Fabrics and Their Ageing Properties, Fibers Polym. 20 (2019) 1347–1359. https://doi.org/10.1007/s12221-019-1078-z.

[34] S.L. Lim, J. Kim, J. Park, S. Kim, J.J. Lee, Electrochemical Deposition of Copper on Polymer Fibers, J. Electrochem. Sci. Technol. 7 (2016) 132–138. https://doi.org/10.5229/JECST.2016.7.2.132.

[35] N. Jaziri, A. Boughamoura, J. Müller, B. Mezghani, F. Tounsi, M. Ismail, A comprehensive review of Thermoelectric Generators: Technologies and common applications, Energy Reports. 6 (2020) 264–287. https://doi.org/10.1016/j.egyr.2019.12.011.

[36] S. Hu, D. Wang, D. Křemanáková, J. Militký, Washable and breathable ultrathin copper-coated nonwoven polyethylene terephthalate (PET) fabric with chlorinated poly-para-xylylene (parylene-C) encapsulation for electromagnetic interference shielding application, Text. Res. J. (2023). https://doi.org/10.1177/00405175231168418.

[37] E. Çinçik, E. Koç, An analysis on air permeability of polyester/viscose blended needle-punched nonwovens, Text. Res. J. 82 (2012) 430–442. https://doi.org/10.1177/0040517511414977/ASSET/IMAGES/LARGE/10.1177_0040517511414977-FIG7.JPEG.

[38] S. Xie, H. Jiang, X. Zhao, X. Deng, Fabrication and performances of high-temperature transient response ITO/In2O3 thin-film thermocouples, J. Mater. Sci. Mater. Electron. 34 (2023) 1–7. https://doi.org/10.1007/S10854-022-09739-9/FIGURES/8.

[39] Z. Zhang, Z. Liu, J. Lei, L. Chen, L. Li, N. Zhao, X. Fang, Y. Ruan, B. Tian, L. Zhao, Flexible thin film thermocouples: From structure, material, fabrication to application, iScience. 26 (2023) 107303. https://doi.org/10.1016/J.ISCI.2023.107303.

[40] Z. Wu, H. Ding, K. Tao, Y. Wei, X. Gui, W. Shi, X. Xie, J. Wu, Ultrasensitive, Stretchable, and Fast-Response Temperature Sensors Based on Hydrogel Films for Wearable Applications, ACS Appl. Mater. Interfaces. 13 (2021) 21854–21864. https://doi.org/10.1021/ACSAMI.1C05291/SUPPL_FILE/AM1C05291_SI_003.MP4.

[41] S. Cruz, G. Azevedo, C. Cano-Raya, N. Manninen, J.C. Viana, Thermoelectric response of a screen printed silver-nickel thermocouple, Mater. Sci. Eng. B. 264 (2021) 114929. https://doi.org/10.1016/J.MSEB.2020.114929.

[42] R.E. Bentley, Handbook of Temperature Measurement Vol. 3: The Theory and Practice of Thermoelectric Thermometry, (1998) 245. https://books.google.com/books/about/Handbook_of_Temperature_Measurement_Vol.html?hl=zh-CN&id=lNvJ_rsUAJkC (toegang verkry 27 Desember 2024).

[43] M. Majdak, M. Jaremkiewicz, The analysis of thermocouple time constants as a function of fluid velocity, Meas. Autom. Monit. 62 (2016) 284–287.

[44] Y. Li, Z. Zhang, X. Hao, W. Yin, A Measurement System for Time Constant of Thermocouple Sensor Based on High Temperature Furnace, Appl. Sci. 2018, Vol. 8, Page 2585. 8 (2018) 2585. https://doi.org/10.3390/APP8122585.

[45] Z. Liu, B. Tian, X. Fan, J. Liu, Z. Zhang, Y. Luo, L. Zhao, Q. Lin, F. Han, Z. Jiang, A temperature sensor based on flexible substrate with ultra-high sensitivity for low temperature measurement, Sensors Actuators A Phys. 315 (2020) 112341. https://doi.org/10.1016/J.SNA.2020.112341.

[46] N. Martiny, A. Rheinfeld, J. Geder, Y. Wang, W. Kraus, A. Jossen, Development of an all kapton-based thin-film thermocouple matrix for in situ temperature measurement in a lithium ion pouch cell, IEEE Sens. J. 14 (2014) 3377–3384. https://doi.org/10.1109/JSEN.2014.2331996.

[47] A. Sheng, S. Khuje, J. Yu, T. Parker, J.Y. Tsai, L. An, Y. Huang, Z. Li, C.G. Zhuang, L. Kester, Q.

Yan, S. Ren, Copper Nanoplates for Printing Flexible High-Temperature Conductors, ACS Appl. Nano Mater. 5 (2022) 4028–4037. https://doi.org/10.1021/ACSANM.2C00019/SUPPL_FILE/AN2C00019_SI_001.PDF.

[48] S. Konishi, A. Hirata, Flexible Temperature Sensor Integrated with Soft Pneumatic Microactuators for Functional Microfingers, Sci. Reports 2019 91. 9 (2019) 1–9. https://doi.org/10.1038/s41598-019-52022-x.

[49] M.M. Mallick, L. Franke, A.G. Rösch, M. Hussein, Z. Long, Y.M. Eggeler, U. Lemmer, High-Sensitivity Flexible Thermocouple Sensor Arrays Via Printing and Photonic Curing, Adv. Funct. Mater. 34 (2024) 1–8. https://doi.org/10.1002/adfm.202301681.

[50] T.N. C. Anderson, Z. H. Fan, J. Richstein, M. Sussman, 2023 IEEE International Conference on Flexible and Printable Sensor Systems, in: 2023 IEEE Int. Conf. Flex. Printable Sens. Syst., IEEE, 2023: bl 1.

[51] T.W. Cheung, T. Liu, M.Y. Yao, Y. Tao, H. Lin, L. Li, Structural development of a flexible textile-based thermocouple temperature sensor, Text. Res. J. 92 (2022) 1682–1693. https://doi.org/10.1177/00405175211057132.

[52] V. Shalini, S. Harish, J. Archana, H. Ikeda, M. Navaneethan, Interface effect and band engineering in Bi2Te3:C and Bi2Te3:Ni-Cu with enhanced thermopower for self-powered wearable thermoelectric generator, Vol. 868. 868 (27833). https://doi.org/10.1016/j.jallcom.2021.158905.

[53] N.P. Klochko, K.S. Klepikova, D.O. Zhadan, V.R. Kopach, S.M. Chernyavskaya, S.I. Petrushenko, S. V. Dukarov, V.M. Lyubov, A.L. Khrypunova, Thermoelectric textile with fibers coated by copper iodide thin films, Thin Solid Films. 704 (2020) 138026. https://doi.org/10.1016/J.TSF.2020.138026.

8 List of papers published by the author

8.1 Publications in journals

[1] **X. Zhang,** Z. Jin, L. Hu, X. Zhou, K. Yang, D. Kremenakova, J. Militky, A Silver Yarn-Incorporated Song Brocade Fabric with Enhanced Electromagnetic Shielding, Materials. 14 (2021) 3779. https://doi.org/10.3390/ma14143779.**(Q1, IF:3.623)**

[2] **X. Zhang**, K. Yang, D. Kremenakova, J. Militky, "Luminous behavior and tensile property of twisted side-emitting polymer optical fibers bundles", Polym. Test., bl 108016, Apr 2023, doi: 10.1016/J.POLYMERTESTING.2023.108016. **(Q1, IF:5.0)**

[3] **X. Zhang**, J. Kallweit, M. Pätzel, K. Yang, D. Kremenakova, J. Wiener, J. Müllerová, M. Tunak, J. Militky, Enhanced side illumination property of end emitting polymer optical fiber (EEPOF)/polyester (PET) woven fabrics by acetone/methanol mixture etching process, Polym. Test. 133 (2024) 108400. https://doi.org/10.1016/j.polymertesting.2024.108400. **(Q1, IF:5.0)**

Journal article: Co-author

[1] K. Yang, M. Venkataraman, **X. Zhang**, J. Wiener, G. Zhu, J. Yao, J. Militky., Review: incorporation of organic PCMs into textiles, Journal of Materials Science. doi: 10.1007/s10853-021-06641-3. **(Q2, IF:4.220)**

[2] K. Yang, M. Venkataraman, J. Wiener, **X. Zhang**, M. Stuchlik, G. Zhu, J. Yao, J. Militky, Crystallization Mechanism of Micro Flake Cu Particle-filled Poly(ethylene glycol) Composites, Thermochim Acta. (2022) 179172. https://doi.org/10.1016/j.tca.2022.179172. (**Q2, IF: 3.378**)

[3] K. Yang, L. Martinkova, O. Ctibor, **X. Zhang**, M. Venkataraman, J. Wiener, G. Zhu, G. Zhang, J. Yao, J. Militky, Mass transfer and thermal buffering effect of hydrophobic fabrics with single-side coating of MPCMs, Prog Org Coat. 172 (2022) 107151. https://doi.org/10.1016/j.porgcoat.2022.107151. (**Q1, IF: 6.206**)

[4] K. Yang, **X. Zhang**, J. Wiener, M. Venkataraman, Y. Wang, G. Zhu, J. Yao, J. Militky, Nanofibrous Membranes in Multilayer Fabrics to Avoid PCM Leakages, Chemnanomat. (2022). https://doi.org/10.1002/cnma.202200352. (**Q2, IF:3.82**)

[5] Yang, K., **Zhang, X**., Venkataraman, M., Wiener, J., Palanisamy, S., Sozcu, S., Tan, X., Kremenakova, D., Zhu, G., Yao, J., & Militky, J. (2023) Structural Analysis of Phase Change Materials (PCMs)/Expanded Graphite (EG) Composites and Their Thermal Behavior under Hot and Humid Conditions *ChemPlusChem*, *88*(4). (**Q1, IF:3.210**)

[6] K. Yang, **X. Zhang**, M. Venkataraman, K. Chen, Y. Wang, J. Wiener, G. Zhu, J. Yao, J. Militky, Thermal behavior of flexible and breathable sandwich fibrous polyethylene glycol (PEG) encapsulations, Text. Res. J. (2024). https://doi.org/10.1177/00405175241236494. (**Q2, IF:1.6**)

[7] K. Yang, **X. Zhang**, M. Venkataraman, J. Wiener, X. Tan, G. Zhu, J. Yao, J. Militky, Sandwich Fibrous PEG Encapsulations for Thermal Energy Storage, ChemPhysChem. (2023). https://doi.org/10.1002/CPHC.202300234 **(Q2, IF:3.238)**

8.2 Contribution in conference proceeding

[1] **X. Zhang**, K. Yang, J. Wiener, M. Venkataraman, G. Zhu, J. Yao, J. Militky, Thermal Behavior of Form-stable Paraffin Wax/Expanded Graphite Composites, in: Textile Bioengineering and [3] Informatics Symposium Proceedings 2022 - 15th Textile Bioengineering and Informatics Symposium, TBIS 2022, 2022. (**Cited in Scopus**)

[2] **X. Zhang,** J. Kallweit, M. Pätzel, D. Kremenakova, J. Wiener, K. Yang, J. Militky, Enhanced Side-Illumination of Etched Polymer Optical Fiber (POF)-Incorporated Woven Polyester (PET) Fabrics, Key Eng. Mater. 977 (2024) 27–33. https://doi.org/10.4028/P-KN4TFJ. Autex 2024

[3] K. Yang, **X. Zhang**, J. Wiener, M. Venkataraman, G. Zhu, J. Yao, J. Militky, Thermal behavior of a multi-layer laminated fabric containing PCMS, in: AUTEX 2022, 2022. https://doi.org/10.34658/9788366741751.64.

[4] S. Palanisamy, V. Tunakova , J . Ornstová, M. Vysanska，M.Tunák，A. Ali，**X. Zhang**，J. Militky, Impact of Bi-axial Stretching of Rib Knitted Fabric on its EMI Shielding, in: Textile Bioengineering and Informatics Symposium Proceedings 2022 - 15th Textile Bioengineering and Informatics Symposium, TBIS 2022, 2022. (**Cited in Scopus**)

[5] K. Yang, **X. Zhang**, J. Wiener, M. Venkataraman, Y. Wang, G. Zhu, J. Yao, J. Militky, Potential of Nanofibrous Membranes in Multi-layer Fabrics to Store PCMs, in: 23rd International Conference STRUTEX, 2022.

8.3 Book chapters

[1] **X. Zhang**, K. Yang, D. Kremenakova, J. Militky, Preparation of Luminous Fabrics by Incorporating Polymer Optical Fibers, Faculty of Textile Engineering, Technical University of Liberec, 2022. (Published in hard copy)

[2] K. Yang, **X. Zhang**, M. Venkataraman, J. Wiener, G. Zhu, J. Yao, J. Militky, Fabrication of PCM fibers: A Mini Review, in: Selected Topics in Fibrous Materials Sciences, Faculty of Textile Engineering, Technical University of Liberec, 2022. (Published in hard copy)

[3] K. Yang, **X. Zhang**, M. Venkataraman, J. Wiener, J. Militky, Characterization of Polymer Crystallization by Using Thermal Analysis, Polym. Cryst. (2023) 13–31. https://doi.org/10.1002/9783527839247.CH2.

[4] K. Yang, **X. Zhang**, M. Venkataraman, J. Wiener, J. Militky J, Phase Change Materials in Textiles for Thermal Regulation. Adv. Struct. Mater. 2023, 201, 27–47. https://doi.org/10.1007/978-981-99-6002-6_2.

8.3 Quotation

Eventual citation of the leading citation databases (Web of Science, Scopus).

Scopus

This author profile is generated by Scopus. Learn more

Zhang, Xiuling

Technická Univerzita v Liberci, Liberec, Czech Republic 57203361354 Connect to ORCID View more

105	20	6	View more metrics
Citations by ***79 documents***	Documents	*h*-index View *h*-graph	

Curriculum Vitae

Xiuling Zhang| Ph.D. student
Faculty of Textile Engineering
Technical University of Liberec
Email: xiuling.zhang@tul.cz

Education

●**Ph.D. in Material Engineering:** 03/2021 – Present
Faculty of Textile Engineering, Technical University of Liberec
Research Topic: Thermoelectric Behavior of Copper-Nickel Coated Polyethylene Terephthalate Fabric
●**M.A. in Textile Materials and Textile Design:** 09/2016 – 03/2019
Zhejiang Sci-Tech University, Hangzhou, China
Research Topic: *Design and Development of Song Brocade Fabric for Shielding NFC Data Reading*
●**B.A. in Textile Engineering:** 09/2012 – 06/2016
Zhejiang Sci-Tech University, Hangzhou, China
Research Topic: Design Research and Practice on Creative Sheer Silk Products

Research Experience

Participated as group leader in Student Grant Competition (SGS) project.

- Thermoelectrical behavior of Ni-Cu-PET layer on fibrous substrate (SGS-2024-6441).
- Enhanced side luminous property of polymer optical fiber-incorporated woven pet fabrics by using acetone/methanol (SGS-2023-6353).
- Structural analysis of polyethylene glycol embedding in expanded graphite under different relative humidity (SGS-2022-6065).

Internship Experience

Fabric Weaving Simulation :12/2015
Elite Textile (Hangzhou) Co., Ltd.
Structural Design of Song Brocade with Fabric CAD: 2016-2018
Suzhou Saintjoy Silk Technical Culture Co., Ltd.
Research on Mechanical Properties of Glass Tapes: 06/2018-09/2018
KMI, Faculty of Textile Engineering, Technical University of Liberec
Surface modification of polymer optical fibers: 09/2022 – 03/2023
Institut für Textiltechnik, RWTH Aachen University

Brief description of the current expertise, research and scientific activities

Doctoral studies	
Studies	Textile Engineering Textile Technics and Materials Engineering full time
Exams	Structure and Properties of Tex. Fibers, 27.07.21 Testing theory and experimental data treatment, 17.12.2021 Heat and Mass Transfer in Porous Media, 19.04.22 Mathematical Statistics 19.05.23 Experimental technique of the textile, 21.11.23
SDE	State Doctoral Exam completed on 29.11.2024 with the overall result passed.
Teaching Activities	
Teaching	-
Leading Bachelors/ Master students	-
Research projects	• Structural analysis of polyethylene glycol embedding in expanded graphite under different relative humidity (SGS-2022-6065), project leader. • Enhanced Side Luminous Property of Polymer Optical Fiber-Incorporated Woven PET Fabrics By using Acetone/Methanol (SGS-2023-6353), project leader. • Thermoelectrical behavior of Ni-Cu-PET layer on fibrous substrate (SGS-2024-6441), project leader.
Other projects	-

Reccomedation of the supervisor

Opinion of the supervisor on Ph.D. thesis of Xiuling Zhang, M.Eng.

Thesis title: **Thermoelectric Behavior of Copper-Nickel Polyethylene Terephthalate Fabric**

The doctoral thesis of student Xiuling Zhang is focused on the preparation and characterization of the properties of a special functionalized textile that exhibits a thermoelectric effect.

As a substrate, the student chose a thin (0.04 to 0.1 mm thick) pointwise thermally bonded porous nonwoven fabric made of fine polyester fibers, which is plated with copper particles (MEFTEX Bochemia comp.). Unlike other solutions, these textiles do not have a compact metallized layer on the surface, but copper and copper oxide particles are fixed on the surface of the fibers, so that porosity and air permeability are maintained on the one hand and flexibility on the other. At the same time, thanks to the perpendicular laying of 2 layers of polyester multifilaments on top of each other (similar to fabrics) and the point thermal bonding, there is low deformability.

The student found a suitable procedure for activating the surface of the textile for attaching nickel nanoparticles, which she practically implemented. She monitored the influence of the nickel deposition time during the plating process on the structure of the resulting layers in terms of composition, morphology, chemical valence states and on the properties of the textile, i.e. porosity, air permeability, electrical and thermal conductivity and resistance and EMI shielding. For comparison, she used copper foil, which was plated with nickel under the same conditions as the mentioned textile.

The student developed a continuous method for measuring the Seebeck coefficient in the dynamic heating mode and compared it with the conventional procedure. She performed measurements of the Seebeck effect including basic statistical evaluation. The student showed that particle systems at the nanoscale have different behavior from the conventional method of manufacturing thermocouples from metals.

The student's diligent work in creating many samples of textiles electroplated with nickel and measuring their thermoelectric effect can be appreciated. Likewise, her publication activities are of an exceptionally good level. Throughout his research tenure at TUL, he has promoted his findings through the publication of 10 papers in journals with high-impact factors (Q1, Q2), 4 book chapters, and 5 articles in conference proceedings. Its h-index is 7. Throughout his academic pursuits, he demonstrated a good level of competency.

During the plagiarism check, less than 4% similarity were found, which was caused by the same declaration used in the introduction of the theses, the description of standardized methods, and the description of the Meftex textile production process.

Overall, I recommend the dissertation for final doctoral defense.

Liberec June 5, 2025 doc Dr. Ing. Dana Křemenáková

Rewievs of the opponents

Opponent review of PhD Thesis

Opponent: Ing. Karel Kupka, PhD.
Dissertation Thesis: Thermoelectric Behavior of Copper-Nickel Polyethylene Terephthalate Fabric
Author: Xiuling Zhang, M.Eng.
Study programme: P0723D270003 Textile Engineering
Thesis Supervisor: doc. Dr. Ing. Dana Křemenáková, Department of material engineering

1. Key Contributions and Novelty

- **Innovative Textile Thermocouple Design:**
  The dissertation presents a novel approach by fabricating a textile thermocouple using a metal–metal junction, achieved by electroplating Ni on a pre-existing Cu-coated PET nonwoven fabric. This strategy is unique compared to conventional thermoelectric textiles based on conducting polymers or semiconductor inks. It offers a robust, flexible, and breathable alternative that is less prone to short-circuiting—thanks in part to the nanoscale distribution of metal particles and the stabilizing influence of inherent copper oxides.

- **Controlled Nanoscale Multilayer Structure:**
  By precisely controlling the Ni deposition time, the work achieves a uniform and compact nanoscale coating that gradually covers the Cu layer and fills the fabric pores. This controlled process not only enhances electrical safety but also contributes to stable thermoelectric performance under mechanical deformations, such as bending, twisting, and even after washing cycles.

- **Custom Measurement Methodology:**
  The dissertation develops and validates a "continuous cooling" test setup that complements the standard controlled temperature method. This dual approach verifies the stability of the Seebeck coefficient (reported in the range of approximately 9–17 μV/K) over a broad temperature difference (up to 110 °C). Although the absolute voltage output is modest, the design's mechanical durability and environmental robustness mark a significant advancement for wearable thermoelectric applications.

- **Multifunctional Textile Properties:**
  In addition to thermoelectric functionality, the Ni@Cu fabric retains high air permeability and exhibits electromagnetic interference (EMI) shielding. These features position the work as an attractive candidate for wearable temperature sensors and other smart textile applications.

---

2. Weak Points, Possible Omissions

- **Low Thermoelectric Efficiency:**
  While the approach provides mechanical robustness and flexibility, the use of two metals (Ni and Cu) inherently results in a low Seebeck coefficient and low power output. The dissertation lacks a detailed discussion on power factor or the dimensionless figure of merit (ZT), making it difficult to benchmark energy-harvesting efficiency against state-of-the-art thermoelectric materials.

- **Inadequate Analysis of Oxide Effects:**
  The formation of copper oxides in the chemically deposited layer is mentioned as beneficial; however, the mechanism by which these oxides influence the net Seebeck coefficient is not

quantitatively analyzed. This leaves open questions regarding the role of unintentional oxide junctions in the overall thermoelectric behavior.

- **Limited Discussion on Long-Term Durability:**
  Although the work includes initial tests for bending, twisting, and washing, there is little detail on the long-term fatigue behavior or cyclic durability under repeated mechanical deformation. Given that durability is a key challenge in wearable devices, more extensive fatigue testing would strengthen the claims.

- **Trade-Offs with Alternative Textile Sensors:**
  The manuscript does not fully address how its performance compares with alternative textile-based temperature sensors (e.g., thermistors) or more advanced printed inorganic thermoelectric generators. A discussion on whether the primary application should be temperature sensing (given the low output) rather than energy harvesting would provide a more balanced perspective.

- **Evaluation, analysis and interpretation of data**
  Statistical methods used throughout the work is generally adequate and acceptable, but basic. The extensive, precise and expensive measurements would deserve more attention and more informative statistics. Among others: Over-using correlation coefficient. Other (and more informative) statistics are recommended instead, such as residual standard deviation, standard deviation of estimated Seeberg coefficient, or its confidence interval. In Section 5.6.3 - Decreased/increased Seebeck coefficients should be tested statistically. At least confidence intervals of S should be computed for each case before claiming differences. (Maybe the differences are insignificant?)

---

3. Comparison with the State-of-the-Art (2000–2025)

- **Material Advances:**
  Recent decades have seen significant progress in both high-performance inorganic TE materials (e.g., nanostructured Bi–Te alloys with ZT >1) and flexible organic thermoelectrics (with ZT improvements through nanostructuring and doping). While these studies emphasize efficiency, they often require rigid or complex multilayer structures. Zhang's work, by contrast, prioritizes wearability and simplicity, aligning with research that focuses on sensor functionality rather than high power output.

- **Wearable Thermoelectrics and Textile Sensors:**
  Prior art such as "Power Felt" and flexible CNT/polymer TEGs have demonstrated higher voltage and power outputs. However, many of these devices sacrifice mechanical flexibility or comfort. Zhang's Ni@Cu fabric, while exhibiting a lower thermoelectric voltage, offers superior durability, breathability, and EMI shielding—all of which are highly desirable in real-world wearable applications.

- **Measurement Methodology:**
  The introduction of a continuous cooling test setup is an innovative contribution. It provides a simpler and effective means of assessing thermoelectric behavior across a broad temperature range, which is critical for wearable applications where the temperature gradient is relatively small.

---

4. Possible Future Directions and Potential Applications

- **Material Optimization:**
  To enhance thermoelectric performance, further work could explore alloying (e.g., using constantan) or introducing semiconductor coatings (such as a thin CuO or CuI layer) to boost the Seebeck coefficient without compromising flexibility. Tailoring the composition to intentionally form metal/oxide junctions may improve voltage output.

- **Scaling via Textile Thermopile Networks:**
  Future research could focus on integrating multiple Ni@Cu junctions in series (e.g., via weaving or knitting techniques) to create textile thermopiles. This strategy would amplify the output voltage, making the device more viable for powering low-energy electronics or self-powered sensors.

- **Integration with Hybrid Energy Systems:**
  Combining the Ni@Cu fabric with other energy-harvesting mechanisms (such as triboelectric or piezoelectric systems) or integrating energy storage elements could transform the textile into a more robust, multifunctional power source for wearable electronics.

- **Enhanced Durability and Real-World Testing:**
  Extending mechanical and environmental testing (including cyclic fatigue and long-term wash durability) will be critical for assessing the device's suitability in everyday wear. Incorporating protective coatings without compromising breathability could further enhance device longevity.

- **Expanded Sensor Applications:**
  Given its stable thermoelectric response and rapid thermal time constant, the fabric shows promise as a temperature sensor for health monitoring, environmental control, or even as a distributed sensor network in smart textiles. Future work might explore real-time temperature mapping across a garment or integration with wireless data acquisition systems.

---

5. Opponent's Questions for the Defender

1. **Regarding Material Efficiency:**
   "Can you elaborate on the trade-offs made by choosing a Ni–Cu pair, especially in terms of thermoelectric efficiency (ZT) and power output, compared to more conventional high-ZT materials used in wearable TEGs? What is ZT, could you determine ZT in your sample"?

2. **On Long-Term Durability:**
   "What are your plans for addressing long-term fatigue and mechanical degradation under repeated bending and washing cycles, and how do you anticipate this will affect the sensor's reliability in everyday use?"

3. **On extending the idea:**
   "What is your view of a weaving technology for producing semi-3D structure (3D scaffold) from 2 metallic or metal-plated conductive yarns (say, Fe - Ni) to built a series of micro-thermocouples with inner and outer side as temperature pools? What is your opinion on other technologies/geometries (3Dprint, successive local metal plating/deposition, Laser scribing). What possible applications do you see?

6. Recommendation for Defense

Overall, the dissertation presents a compelling and innovative approach to wearable thermoelectric textiles. The fabrication method, which emphasizes scalability, flexibility, and environmental robustness, is highly commendable. Stated aims and objectives were fulfilled and appropriate methodology was developed and applied. This work represents a valuable contribution to the field of wearable thermoelectrics and offers significant potential for practical applications in smart textiles.

I recommend that the candidate is allowed to defend her dissertation thesis.

Reviewer: Ing. Karel Kupka, PhD. & PhD.

Pardubice, 30. 3. 2025

Prof. Ing. Čestmír Drašar, Dr.
University of Pardubice
Faculty of chemical technology
53210 Pardubice
Czech Republic

UNIVERZITA PARDUBICE
FAKULTA CHEMICKO-TECHNOLOGICKÁ

Review of the dissertation

"Thermoelectric behavior of Copper-Nickel polyethylene terephthalate Fabric"

by

Xiuling Zhang, M.Eng.

This dissertation focuses on the textile-based thermoelectric (TE) materials. The material part of research is based on polyethylene terephthalate (PET) fabric, that is electroplated with a metallic layer. Commercially available chemically copper-plated fabric is used as the starting material (precursor). The fabric is electroplated by copper to obtain thicker plating a by nickel to prepare a thermoelectric (TE) couple that can be used as a TE generator.

The thesis follows the traditional format, beginning with short introduction and state-of-the-art sections, followed by experimental and results and discussion sections. The thesis contains lists of symbols and abbreviations, unfortunately not in alphabetical order. The "Aim and Objectives" section indicates the technological nature of the thesis: the development and optimization of the plating process and the characterization of the prepared plated fabric using many physicochemical methods. The chosen methods were relevant to the studied technical parameters. The thesis presents a significant amount of new and valuable data from a textile technology standpoint. The writing is generally good and clear, but it is overly verbose in many places. In addition in "scientific" parts it fails to explain the point often merely due to improper terms, e.g. what is "TE phenomena"(45) "electron carriers"(46)... The discussion of the characterization data is mostly accurate. Below are some important points of concern that should be considered.

1) The TE properties were of special interest, as indicated by the title. Two methods were developed to measure the primary TE parameter, the Seebeck coefficient. Together with electrical conductivity, the TE power factor was evaluated. The TE performance of the prepared TE fabric is poor. However, it can be optimized further. Unfortunately, it remains unclear exactly how the prepared "TE" fabric can be used for generation, the apparent main goal. The prepared TE structure appears difficult to apply. This leaves readers puzzled about the motivation behind such a TE fabric. The electroplating process has been developed and applied successfully. However, none of the sections adequately address the main goal of the TE applications. This is the most serious drawback of the thesis and a missed research opportunity.
2) There are several technical/scientific points to be addressed.
   a. p. 16, the author suggests comparing Cu/Ni plated fabric with Ni plated copper foil. It is a good idea providing that the plated metal layers are of comparable thickness and metal ratios $R_{Ni/Cu}$, which is not the case. Is it still a reasonable comparison? On the same page, what is the reason using exactly 1 cm wide samples?
   b. p. 18, the term D-space is not defined; is it an atomic planes distance?

(tel. +420466036036, mob. +420737933342, e-mail: cestmir.drasar@upce.cz)

c. p. 20, the equation 4.5 seems to be incorrect, please comment on it.
d. p. 24, fig. 4.3, the cold plate ("temperature-controlled insulated material" mentioned on p. 22) is missing. In addition, the figure caption is poor reading just "Thermoelectrical measurement with continuous colling model" with no comments what is shown in the figure, that is why the cold plate is not "missing".
e. The figure and table captions should be complete/self-explanatory in general.
f. p. 27, fig. 5.3, figs c and e are incorrect. I think that the marks are reversed twice. What is the correct version?
g. p. 36, fig. 5.10, figure A) contradicts the figure B) or vice versa. The relative changes differ significantly between these figures.
h. p. 40, figure 5.12, linear and exponential functions are used arbitrarily. What is the theoretical prediction/assumption?
i. p. 43, figure 5.14 and 5.15, the figure is difficult to analyze, but the Seebeck coefficient, S of a material is defined at a given temperature. How did you derive S from the curves?
j. p. 45, figure 5.16, it is not a TE phenomenon, it is an explanation of S for a composite due to a shortcut. It is not correctly explained. Where exactly do the shortcut currents flow?
k. p. 46, figure 5.17, the statement "...porous architecture effectively minimizes electron carrier shortcuts..." is not explained on the microscopic level. I do not see now how can this be true regarding the figure 5.17.
l. The comparison starting on p. 56 is unreasonable, when the particular TE structure is unknown. The Seebeck value is not enough. Can you compare your material with any of that published for a particular TE structure?
m. Have you tried using a more acidic solution for electroplating? It would generate more hydrogen, which could help to reduce the oxides in the prepared layers. What are the limits for PET?

The "Future scope and work" section is very general providing the reader with no clear outlook. There is one exception, however. The author suggests investigating copper oxide-based TE fabric. This could result into much higher TE performance, although the mechanical properties would probably be inferior to those of metals. This idea could work if the **proper structure** of the TE fabric is developed. Do you have any idea how to proceed?

The thesis is seemingly supported by a number of original scientific articles with significant author participation. Which papers specifically summarize the thesis, though?

All raised issues and comments should be addressed consistently within the defense.

I mentioned some significant objections to the thesis above. Nevertheless,

I recommend defending this thesis.

Pardubice 20. 05. 2025

Prof. Ing. Čestmír Drašar, Dr.

(tel. +420466036036, mob. +420737933342, e-mail: cestmir.drasar@upce.cz)